Carbohydrate Polymers 365 (2025) 123792

Contents lists available at ScienceDirect

Carbohydrate Polymers

journal homepage: www.elsevier.com/locate/carbpol

Breaking free from PFAS: biocompatible, durable and high-performance octenyl succinic anhydride (OSA)-modified starch/chitosan coating with ZnO for textile applications

Anja Verbič [a], Blaž Stres [a,b,c,d], Ivan Jerman [e], Barbara Golja [a,f], Ema Žagar [g], Vuk Martinović [a], Petja Logar [a], Gregor Lavrič [a,h], Anže Prašnikar [a], Blaž Likozar [a], Uroš Novak [a], Ana Oberlintner [a,*]

[a] Department of Catalysis and Chemical Reaction Engineering, National Institute of Chemistry, Hajdrihova 19, 1000 Ljubljana, Slovenia
[b] Jožef Stefan Institute, Department of Automation, Biocybernetics and Robotics, Jamova cesta 39, Ljubljana, Slovenia
[c] Faculty of Civil and Geodetic Engineering, Institute of Sanitary Engineering, Jamova 2, Ljubljana, Slovenia
[d] University of Ljubljana, Biotechnical Faculty, Jamnikarjeva 101, Ljubljana, Slovenia
[e] Laboratory for Coating Development, Department of Materials Chemistry, National Institute of Chemistry, Hajdrihova 19, 1000 Ljubljana, Slovenia
[f] Department of Textiles, Graphic Arts and Design, Faculty of Natural Sciences and Engineering, University of Ljubljana, Aškerčeva 12, 1000 Ljubljana, Slovenia
[g] Department of Polymer Chemistry and Technology, National Institute of Chemistry, Hajdrihova 19, 1000 Ljubljana, Slovenia
[h] Pulp and Paper Institute, Bogišićeva 8, 1000 Ljubljana, Slovenia

ARTICLE INFO

Keywords:
Chitosan
Octenyl succinic anhydride
Modified starch
Biopolymer
Hydrophobic coating
Functional textile

ABSTRACT

The development of textile coatings as alternatives to *per-* and polyfluoroalkyl substances (PFAS) is a high priority due to global regulatory efforts aiming to phase out PFAS, driven by alarming environmental contamination and significant human health concerns. To address the urgent need for replacements, this research develops a health-friendly hydrophobic coating for two of the most common textile substrates, cotton and polyester. The developed coating, consisting of chitosan matrix and octenyl succinic anhydride-modified starch in synergy with ZnO, achieved water contact angles up to 132°. A successful transition to industrial application provided a translucent and homogeneous hydrophobic protection, without noticeably affecting the material's physical properties. Maintained or improved mechanical properties, supported by FTIR analysis, indicate a benign coating process that provides fiber reinforcement. Durability is demonstrated through multiple washing cycles without decrease in hydrophobicity, and high abrasion resistance (min. 20,000 cycles), winning against its commercial fluorinated counterpart. The water-repellent properties show stability over a longer period of time (min. 230 days). The biodegradability study confirmed the environmental compatibility as the biopolymer coating decomposed in 8 days. Finally, multivariate statistical analysis determined an optimal coating process to ensure effective integration of the newly developed sustainable coating into textile manufacturing processes.

1. Introduction

The use of poly- and perfluoroalkyl substances (PFAS) is widespread in various industries, most commonly in aviation, biotechnology, packaging, food industry, cosmetic products, pesticides, and textile production (Glüge et al., 2020). Approximately 15,000 substances are currently classified under this term, (2022a; CompTox, 2022b) and leach into the environment, including drinking water, at all stages of their life cycle (Ackerman Grunfeld et al., 2024; Høisæter & Breedveld, 2022). Studies have shown that PFAS exposure is associated with various negative health effects, including cancer, thyroid disease, reduced fertility, and developmental and metabolic problems (Bartell & Vieira, 2021; Blake et al., 2018; Fenton et al., 2021; Panieri et al., 2022; US EPA 2021), highlighting the urgent need to replace them. With studies demonstrating their long-term stability, bioaccumulation and negative impacts on human health and the environment, the banning and phasing out of PFAS in the European Union began in 2009 with the ban on perfluorooctane sulfonic acid, followed by perfluorooctanoic acid in 2019 and perfluorohexane sulfonic acid in 2022 under the Stockholm Convention (UNEP, 2009, 2019, 2022). Initiatives aim to

* Corresponding author.
E-mail address: ana.oberlintner@ki.si (A. Oberlintner).

https://doi.org/10.1016/j.carbpol.2025.123792
Received 27 January 2025; Received in revised form 14 May 2025; Accepted 22 May 2025
Available online 25 May 2025

eliminate PFAS altogether, with the European Chemical Agency proposing to restrict or ban up to 12,000 compounds (Spyrakis & Dragani, 2023), and New York prohibiting the sale of apparel with intentionally added PFAS (Department of Environmental Conservation, 2025). In 2023, authorities of Denmark, Germany, Sweden, the Netherlands and Norway have proposed banning or restricting approximately 10,000 PFAS compounds (ECHA, 2023), creating space for alternatives. Current hydrophobic alternatives to PFAS, such as hydrocarbon polymers, alkylamines and acrylates, have their drawbacks, such as difficulties in matching performance, or replacing one harmful chemical with another that poses comparable health risks. Similarly, melamine is being used as a PFAS alternative, however several studies have linked it to urinary tract cancer, leading to its recent recommendation for inclusion on the REACH list (Zheng & Salamova, 2020). Eliminating the use of all fluorinated chemicals, has thus been unsuccessful to this date, enabling these "forever chemicals" to further endanger ecosystems and human health. One of the main contributors to the concerning problem is the textile industry, where PFAS are mainly used to impart hydrophobicity to the materials used in wearable textiles. Overcoming this challenge requires innovative approaches, such as the application of surface treatments or coatings that enhance the hydrophobic properties while maintaining the breathability and comfort of the fabric. Several strategies, such as the use of covalent organic frameworks (Mullangi et al., 2017), water-based polyurethane (Dai et al., 2021), fluorinated and quaternary ammonium-functionalized silica nanoparticles in combination with polydimethylsiloxane (Ye et al., 2021), plasma treatment (Oberlintner et al., 2024; Samanta et al., 2016, 2021) have been employed.

On the other hand, nature has succeeded in designing remarkable (super)hydrophobic materials and structures, with the most prominent being lotus leaves, duck feathers, butterfly wings, rose petals, and mosquito eyes, that serve as an inspiration in the search for sustainable PFAS replacements (Barthlott & Neinhuis, 1997; Byun et al., 2009; Land & Nilsson, 2012; Saji, 2020). Their wettability properties are due to a unique interplay between low surface energy, determined by surface chemistry, and surface micro- and nanostructure. Renewable plant (carnauba, jojoba, sunflower, and rice bran) and animal-derived (beeswax, shellac, wool and spermaceti) waxes are commercially applied and extensively studied as one of the most common tools to achieve low surface energy and create suitable surface structure (Bashari et al., 2020; Forsman et al., 2017, Forsman et al., 2020; B.-Y. Liu et al., 2019; Singh et al., 2023). However, they tend to clog the pores of the textile, leaving little room for the highly important breathability (Forsman et al., 2020). Another approach to hydrophobicity is the use of biopolymers (cellulose, starch and chitosan) and proteins (zein and hydrophobin) (Gonçalves et al., 2020; Opwis & Gutmann, 2011; Shahid et al., 2022). While cellulose, alginate and starch are naturally hydrophilic and have to be modified to achieve the desired properties (Cheng et al., 2018; Cunha & Gandini, 2010; Lin et al., 2024; Oberlintner et al., 2021; Zhang et al., 2022), chitosan films and coatings already exhibit a certain degree of hydrophobicity (Lavrič et al., 2021). Chitosan represents a perfect coating matrix due to its viscosity, surface tension, adhesive strength and mechanical properties (Hahn et al., 2019). Furthermore, it is widely available, relatively low cost, non-toxic, insoluble in water, biodegradable, and allows surface modification, as well as film formation, making it a top choice for alternative hydrophobic coatings (Bajić et al., 2019). With this in mind, several studies have exploited the advantages of chitosan to develop (super)hydrophobic coatings. Examples include modification of chitosan with long-chain polymers, adsorption of anionic surfactant on chitosan surface, surface hydrophobization by plasma, or through esterification (Ivanova & Philipchenko, 2012; Oberlintner et al., 2022; Roy et al., 2022; Tagliaro et al., 2024). OSA-modified starch is hydrophobic due to the low polarity of OSA and long chains that hinder water (Altuna et al., 2018; Lu et al., 2020), food-grade safe, low cost, and commonly used for stabilizing emulsions (Fan et al., 2025; Wang et al., 2025; Yan et al., 2019). At low pH, its free carboxyl groups on the surface become negatively charged, allowing the formation of a stable polyelectrolyte complex through electrostatic interactions with cationic chitosan (Wang et al., 2025). Such a complex combines the best of both worlds – the chitosan's suitability for coating application and the hydrophobicity of OSA-modified starch. Inorganic zinc oxide (ZnO) particles, which are believed to improve water resistance behavior through structuring the surface and increasing its roughness (Verbič et al., 2019), were added to the coating. The increase in surface roughness through the creation of hierarchical structures, enables the air trapping ability of the samples. By introducing ZnO nanoparticles into the coating dispersion we aimed to provide an additional structural modification to increase hydrophobicity, different from the chemical hydrophobicity imparted by chitosan and modified starch. While functional groups in chitosan and OSA-modified starch might contribute to chemical hydrophobicity by repelling water molecules, additional ZnO nanoparticles could enhance the effect by providing microscale and nanoscale roughness, complementing the chitosan/OSA-starch effect. ZnO is widely used in the various industries due to its multifunctional properties. In cosmetics they serve as UV filters in sunscreens and antimicrobial agents. In textiles, they provide functional finishes with UV protection, antimicrobial or self-cleaning properties (Verbič et al., 2019). It is listed as Generally Recognized as Safe (GRAS) by the US Food and Drug Administration (FDA, 2025a) and is used as a color and nutritional supplement (FDA, 2025b). At the same time, its use requires careful consideration, especially in regard to concentration and particle size. While higher concentrations of ZnO particles may optimize the performance of the material, the direct exposure to ZnO nanoparticles could cause oxidative stress, cytotoxicity and inflammation (De Berardis et al., 2010; Zhuo et al., 2024). While in theory, nano-sized ZnO particles could exhibit greater toxicity than larger particles due to their increased surface area and enhanced reactivity, some studies have confirmed the increased toxicity with the decreasing size (Kaya et al., 2016), while others have rejected this and found the opposite (Kim et al., 2024; Mitjans et al., 2023).

In frame of this research, we hypothesized that a biopolymer-based coating composed of OSA-modified starch, chitosan, and ZnO particles would exhibit hydrophobicity, durability, and stability comparable to PFAS, thus representing a new class of sustainable coatings. Aiming to minimize its potential toxicity while still benefiting from its structural properties, very low concentrations of ZnO were included (< 0.10 wt%). Additionally, we have tested different particle sizes (from micro to nano) to evaluate their effect on surface roughness, hydrophobicity and overall material performance. This way we aimed to find the optimal balance between functionality and safety. While the previous research has focused on the development of films or composites and achieving hydrophobicity, our research focused on the practical application of the newly developed coating on two different textile substrates (cotton fabric as a natural cellulosic material, and polyester fabric as a synthetic material), scaling up the application process from laboratory scale to hand-operated industrial application technique and analyzing the functional properties and durability of the material. To confirm this, starch was modified with OSA, incorporated into a chitosan matrix and applied as a coating to improve the hydrophobicity of cotton and polyester textiles, shedding a new light on the use of OSA-modified starch, an established emulsifier and stabilizer in the food and beverage industry (Zhao et al., 2018). The coating provided hydrophobicity, suitable mechanical properties, prolonged stability, and high durability. With statistical analysis including textile functionality and process scale-up, this study offers an optimal coating procedure, bringing such bio-based fluorine-free coating one step closer to commercial applications.

2. Materials and methods

2.1. Materials

Chitosan (CAS 9012-76-4, medium molecular weight, Mw = 950 kg mol^{-1}, Mn = 250 kg mol^{-1}, Đ = 3.82, 76 % deacetylated) (Fig. S1, Table S1), starch from corn (unmodified, CAS 9005-25-8, pure amylopectin, amylose in traces, pH 5.6, moisture content 10.5 %, Mw x 10^6 = 12.9 g mol^{-1}, Mn x 10^6 = 6.9 g mol-1, Đ = 1.87) (Fig. S2, Table S2), 2-octenylsuccinic anhydride (cis and trans)(OSA), acetic acid, ethanol absolute (99.5 %), ZnO nanoparticles in three different sizes (< 50 nm, < 100 nm, < 5 μm) were purchased from Sigma Aldrich (St, Louis, Missouri, US). Commercially available flourine-containing hydrophobic coating (referred to as PFAS throughout the manuscript) Nitoguard textile (Mavro International, Zaltbommel, Netherlands) was used as a benchmark coating. Plain weaved cotton fabric (CO) was purchased from Europrint (Ajdovščina, Slovenia) and polyester (PES) fabric from Svet Metraže (Ljubljana, Slovenia). HCl (Pregl chemicals, Ljubljana, Slovenia) and NaOH (Merck, New Jersey, US), were used for pH adjustment during starch modification.

2.2. Methods

2.2.1. Starch modification and its characterization

35 wt% of waxy corn starch was dissolved in water at 35 °C (the temperature was regulated through water bath) on magnetic stirrer at 400 rpm with pH maintained at 8.5 using 0.5 M NaOH. After complete dissolution (approximately 30 min), the solution was cooled to room temperature. OSA was added dropwise in amounts to reach 3 wt%, 6 wt % and 9 wt% with respect to mass of starch over a time frame of 1 h under constant stirring, while keeping the pH constant. The reaction was stopped after 2 h by adding 0.5 M HCl and adjusting the pH to 6.0. The modified starch was then washed twice with distilled water and twice with anhydrous ethanol in consecutive cycles with intermittent centrifugation at 4500 rpm for 10 min. The precipitate was then dried in a ventilated oven (Kambič, Slovenia) at 40 °C overnight. The samples were labeled as OSA—S3, OSA—S6 and OSA—S9 indicating concentrations of 3, 6, and 9 %, respectively. The degree of substitution (DS) was determined by titration, according to a previously described protocol (Plate et al., 2012).

2.2.2. Preparation of coatings dispersions and coating procedure

Chitosan was dissolved in 1 *v*/v % acetic acid at concentrations of 0.66, 0.5, and 0.22 wt% on a stirring plate overnight at room temperature. Dried OSA-starch with different DS (final coating dispersions were labeled CH—OSA—S3, CH—OSA—S6, and CH—OSA—S9) was added to the dispersions at three different chitosan:OSA-starch ratios (1:3, 1:6, 1:9). Three different sizes of ZnO (< 50 nm, < 100 nm, < 5 μm) were added to the coating dispersions at concentrations of 0.66, 0.50, 0.22 and 0.10 wt%. The coating was mixed well and coated with two different procedures: spray coating and dip-pad-dry process. Both types of textiles (CO and PES) were coated. Uncoated fabrics were used as a control. On laboratory scale, the coating was applied by using a spray bottle filled with 5 mL of dispersion and sprayed homogeneously over the 10 × 10 cm (10 cm in weft direction /width, 10 cm in warp direction/length) fabric piece dried in a ventilated oven (Kambič, Slovenia) at 40 °C for 30 min. The procedure was repeated 3 times, with the last drying step lasting 16 h. The scaled-up samples, approximately 35 × 40 cm in size (35 cm in weft direction/width, 40 cm in warp direction/length), were prepared by immersing the fabric samples in a glass impregnation bath containing coating dispersion for 1 min, wringing on a double roller foulard with a wet pick-up of 80 %, and drying in a laboratory continuous dryer (Mathis, Switzerland) for 5 min at 40 °C. Three sets of samples were prepared by applying the coating material 1, 2 and 3 times to each sample, labeled UP1, UP2 and UP3, respectively. The samples that received multiple coatings were thoroughly dried (for 5 min at 40 °C) between each application to ensure optimal adhesion and uniformity of the coating layers.

To benchmark biopolymer-based coatings dispersion developed in frame of this study, a commercial PFAS-containing coating was used. Fabric samples were dip-coated according to the instructions provided in product's Safety data sheet. The CO and PES fabrics were immersed in a glass impregnation bath containing undiluted coating for 1 min, wringed on a double roller foulard (Mathis, Switzerland) with a wet pick-up of 80 % and dried in a laboratory continuous dryer (Mathis, Switzerland) at 150 °C for 2 min.

2.2.3. Surface wettability

The first indication of the success in hydrophobization of the textiles was evaluated by measuring the water contact angle (WCA). For this analysis, tensiometer Theta T200 (Biolab Scientific, Gothenburg, Sweden) was used. The water drop was 3 μL and the measurement was taken at 5 s after the start of the measurement. To analyze the stability of chitosan coating alone, the measurements were performed at 5, 10, 15 and 20 s. For selected formulations with the highest WCA, the potential absorption of a water droplet was followed over the course of 5 min.

2.2.4. Scanning electron microscopy (SEM) and energy dispersive spectroscopy (EDS)

The surface morphology of the control (untreated) and coated CO and PES samples was analyzed using a SUPRA35 VP scanning electron microscope (Carl Zeiss, Germany), with a primary electron beam accelerating voltage of 1 kV, an aperture of 30 μm and a working distance of 6.1 mm. The micrographs were taken at 150× and 1000× and 50,000× magnification.

The presence of zinc and fluorine on the textile samples was determined by EDS (Oxford Instruments Ultim Max 100 silicon drift detector (SDD)) at 20 kV with 120 μm aperture at 8.5 mm working distance. The analysis was performed at three locations for each textile sample and the average value was reported. To achieve sample conductivity, the samples were coated with a 6 nm of layer of gold prior to the analyses.

2.2.5. ATR-FTIR analysis

ATR-FTIR was used to study into structural changes in OSA-starch and coated textiles. Perkin Elmer (Massachusetts, USA) Omega 3 was used, with measurements between 4000 cm^{-1} and 400 cm^{-1} with a resolution of 1 cm^{-1} and an accumulation of 16 scans. The measurements were repeated at three separate points of the sample and the average was reported. Modified starch (OSA—9), chitosan (CH), and the developed coating consisting of chitosan matrix, modified starch and ZnO particles (CH + OSA-9 + ZnO) were measured as solid-state films/particles. Other samples (CO, CO PFAS, CO UP1, CO UP2, CO UP3, PES; PES PFAS, PES UP1, PES UP2, PES UP3) were analyzed as textiles.

2.2.6. Mechanical properties

Breaking strength (N) and elongation (%) of untreated and coated CO and PES samples were analyzed using the Zwick Roell Z010 in according to standard ISO 13934–1:2013 with slight modifications. Each sample was cut three times in the warp and weft directions (250 mm × 50 mm) and analyzed using a pre-loading of 2 N and a speed of 200 mm/min. Before the measurements, the samples were conditioned at 23 °C and 50 % relative air humidity for 24 h. The breaking strength and elongation were read at the breaking point of the test sample and the average and standard deviation were calculated.

2.2.7. Stiffness of the samples

The bending rigidity (G) of the samples was measured by performing "Shirley" stiffness test according to ASTM standard D-1388-64, which assesses how the sample bends under its own weight. Specimens (25 × 200 mm in size) were cut in both warp and weft direction (5 samples per direction) and conditioned in a controlled atmosphere at 65 ± 2 % relative humidity and 20 ± 1 °C for 24 h. Each specimen was extended

from the horizontal surface at a controlled rate in a direction parallel to its long dimension, until its leading edge projected from the edge of a horizontal surface. The overhang length was measured when the tip of the specimen depressed under its own weight to form a 41.5° angle. From this length the rigidity was calculated according to the following equations:

Rigidity in warp and weft direction:

$$G_{1(2)} = T \times \left(\frac{l_{1(2)}}{2}\right)^3,$$

where the T is fabric weight per unit area *(g/m²)* and l is bending length (cm).

Overall rigidity:

$$G = \sqrt{G_1 \times G_2},$$

Where G_1 and G_2 are bending rigidities (mg cm), in warp and weft directions.

2.2.8. Thickness

Thickness of the coated samples was measured with digital caliper Mitutoyo ID-C112X (Mitutoyo, Japan) with an eight mm stem diameter and ≤ 1.5 N measuring force. Five measurements of each sample were performed and the average value was reported.

2.2.9. Fabric mass per unit area

The fabric mass per unit area was determined according to SIST-EN 12127 standard which describes methods for measuring mass of small samples in the standard atmosphere. Five specimens of each sample were cut to a size of 10 × 10 cm (100cm^2), weighed and then the mass in grams per 100 cm^2 was recalculated to mass in grams per m^2.

2.2.10. Color measurements

The color of the samples was determined by measuring the reflectance using a Spectro 1050 spectrophotometer (Datacolor, Switzerland) according to the SIST EN ISO 105-J01 standard (General principles for measurement of surface color), from which the CIE L*a*b* color coordinates and the color strength (K/S value) were calculated. Five measurements of each sample were performed using a 6.6 mm aperture and the average value was calculated by the Datacolor TOOLS plus computer software.

2.2.11. Thermal stability

Thermogravimetric analysis (EGA 4000, Perkin Elmer, USA) was performed to evaluate the thermal stability of the coating. Approximately 50 mg of the coated textile sample was heated from 40 °C to 800 °C at a rate of 5 °C per minute in a nitrogen atmosphere.

2.2.12. Abrasion resistance

The abrasion resistance of the samples was determined using the Martindale abrasion testing apparatus M235 (SDL International, UK) according to SIST EN ISO 12947–2:1999 standard. Two sets of biopolymer-coated and PFAS coated samples with a 38 mm diameter were subjected to rubbing cycles of 1000, 5000, 10,000 and 20,000. The WCA of the rubbed samples was measured afterwards.

2.2.13. Washing durability

Resistance to washing was determined according to the ISO 105-C06 standard, using the Gyrowash 815 apparatus (James Heal, UK). A simulation of one and five domestic washing cycles was performed by conducting A1S and A1M tests. All washings were performed by immersing the samples (10 × 4 cm) in 150 mL of 4 g/L ECE phosphate reference detergent B solution (SDC Enterprises Limited, UK), with the addition of 10 stainless steel balls. The samples were washed at 40 °C for 30 min (simulation of one domestic washing cycle) and for 45 min (simulation of five domestic washing cycles). After the completed washing, the samples were rinsed twice for one minute in a 100 mL of Milli-Q water, squeezed, and dried at room temperature.

2.2.14. Multivariate statistical analysis

The data derived from the measurements of characteristics described in this paper were utilized in multivariate statistical analysis as outlined in Oliveri et al. (2020). The data were first organized into matrices and Box-Cox transformed as described previously (Vidmar et al., 2023). For clustering, Euclidean, Bray-Curtis and Occhiai distances were used with Paired group or Ward's method was utilized in parallel (Cophenetic correlation = 0.981; Number of bootstraps = 1000) as described before (Peres-Neto et al., 2006; Smith & Lundholm, 2010; Stres et al., 2013) in PAST (Hammer et al., 2001).

Results and discussion

2.3. Developing the optimal formulation

In this study, a chitosan/modified starch-based alternative to PFAS hydrophobic coatings was developed and optimized. Several parameters were tested to obtain the most suitable coating solution, including the composition of the chitosan base, the degree of starch modification, the ratio between the two biopolymers, and the ZnO loading and particle size.

First, to find the optimal composition of the chitosan matrix, three different concentrations of chitosan (0.22, 0.5 and 0.66 wt%) dissolved in acetic acid were coated on cotton. Higher concentrations, especially 0.66 wt% resulted in a dispersion that was too viscous to ensure a homogeneous coating. Furthermore, concentrations of 0.5 wt% and 0.66 wt% did not surpass the hydrophobic threshold, exhibiting WCA of 70 ± 5° and 65 ± 13°, respectively (Fig. S3). Therefore, 0.22 wt% chitosan solution (WCA 86 ± 9° on CO fabric and 46 ± 11° on PES) was selected and used as the matrix for further experiments. While the chitosan-coated CO and PES fabric initially showed high WCA, these values dropped significantly within 10 s and showed high variability between measurements (Fig. S4). Building on these findings, we further investigated the effect of incorporating starch into the matrix. Modification of starch with OSA facilitates the substitution of hydroxyl groups on starch with hydrophobic octenyl groups, resulting in a decrease in the free surface energy, as well as hindering the starch backbone from the water molecule, and thus reducing wettability (Bai & Shi, 2011; Trubiano, 1986). The successful modification was confirmed by ATR-FTIR analysis (Fig. S4), where newly emerged peaks at 1730 cm^{-1} are visible, as well as by titration and DS determination. The DS obtained were 0.009 ± 0.0009 %, 0.015 ± 0.0016 %, and 0.025 ± 0.0009 % for samples OSA—S3, OSA—S6, and OSA—S9, respectively (Table S3). Both fabrics coated with unmodified starch exhibited hydrophilic properties, while in others a proportional increase in WCA with respect to DS was observed, indicating that the samples became progressively more hydrophobic as the degree of starch modification increased. This was particularly evident for the PES fabrics, which exhibited a WCA of 109 ± 10° when treated with CH—OSA—S9, compared to values just below 95° for CH—OSA—S6 and CH—OSA—S3 (Fig. 1a). A similar trend, however with a smaller difference, was observed for the CO fabric, where WCA decreased from 119 ± 6° when coated with CH—OSA—S9 to 112 ± 5° and 111 ± 3° for CH—OSA—S6 and CH—OSA—S3. This suggests that the degree of starch modification plays a crucial role in altering the surface properties of the fabrics, thereby improving their resistance to water absorption. Finally, to explore the interactions between chitosan and modified starch and to gain insight into their combined effects on fabric wettability properties, the optimal synergy between coating components was determined by testing three different ratios of chitosan to modified starch: 1:3, 1:6, and 1:9 using OSA—S9. The highest WCA was observed with the 1:3 ratio on both CO (119 ± 6°) and PES (109 ± 10°) fabrics, while a higher amount of modified starch relative to chitosan resulted in the opposite effect (Fig. 1b). Although

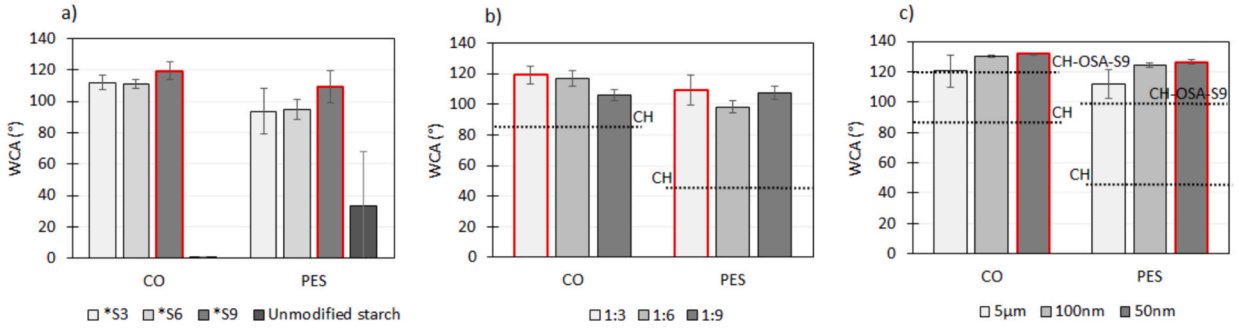

Fig. 1. WCA of laboratory-scale coated CO and PES samples with a) unmodified starch and starch modified to different DS (*denotes OSA-CH-), b) varying ratio between chitosan and modified starch, c) added ZnO particles of different average size.

OSA-starch increases the hydrophobicity of the chitosan matrix through the formation of chitosan/OSA-starch complexes, it does not exhibit hydrophobic properties when coated on the fabric itself (Fig. S5), therefore coatings where modified starch greatly outweighs chitosan (chitosan to starch ratio 1:6 and 1:9) exhibit reduced hydrophobicity. The determined optimal chitosan to starch ratio and DS of starch ensures hydrophobic properties of the treated fabrics and further opens up new possibilities for the development of functional textiles, therefore we investigated the improvement of textile performance by incorporating inorganic particles.

ZnO particles of different sizes (< 50 nm, < 100 nm, and < 5 μm) were added to the most optimal coating (CH—OSA—S9 coating with chitosan to starch ratio 1:3) to tailor the surface morphology and thus further improve the water-repellency as well as other properties of the samples (Fig. 1c). It is generally known that smaller particles have higher volume-to-surface ratio which increases their reactivity (Saleem & Zaidi, 2020). However, we have noticed a correlation between the particle size and the hydrophobicity. As shown in Fig. 1c, smaller particles, particularly those on the nanoscale, have a positive effect on hydrophobicity. By decreasing the ZnO particle size from <5 μm to <100 nm, the WCA values increase from 121 ± 11° to 130 ± 1° for CO and from 112 ± 10° to 124 ± 1° for PES fabric. When the ZnO size is reduced to <50 nm, the WCA further increases to 132 ± 0° for CO and 126 ± 2° for PES. The increase in WCA may be due to the increase in surface roughness achieved by the addition of ZnO in the coating (Ghasemi et al., 2018; Shahid et al., 2022), in particular, the smallest size of ZnO particles, where higher surface roughness could be achieved. It seems that the smaller ZnO particle size also contributed to a lower standard deviation (from 10.5 (CO) and 9.6 (PES) with <5 μm particles, to 0.2 (CO) and 1.6 (PES) with <50 nm particles) between measurements of WCA between samples, thereby improving the uniformity of the samples. Finally, by testing several different concentrations of ZnO, varying from 0.66 wt% to 0.1 wt%, the optimal concentration of ZnO was found to be the lowest (achieving WCA of 121 ± 10° on CO and 112 ± 10° for PES), which is desirable from an environmental and economic point of view. Higher concentrations of ZnO (0.66 and 0.5 wt%) resulted in a significantly increased viscosity of the coating dispersion, possibly due to aggregation of the ZnO particles, making it unsuitable for spray coating application.

2.4. From lab-scale to pilot-scale

To investigate the scalability and applicability of the developed formulation, a pilot scale dip-pad-dry application process was used. To demonstrate the competitiveness of the novel bio-based coating, a comprehensive comparison with a commercial PFAS-containing coating was performed. To gain insight into the effect of layering during scale-up, one, two, or three layers (UP1, UP2, UP3) of coating were applied. The results indicated that the wettability was not dependent on the number of passes through the coating process with all the samples exhibiting WCA around 125° for both CO and PES (Fig. 2a and b). Although the process involved wringing on a double cylinder foulard, which could potentially remove a significant amount of the coating from the samples, good hydrophobicity was achieved as further shown in Video S1 and Video S2. To test the wettability to a wider range of common liquids, tea, milk, coffee and juice were dropped on the surface, revealing resistance to all of them (Fig. 2c). Additionally, the dynamic wettability of the control, chitosan-coated, scaled-up sample (UP1) and PFAS-coated samples were determined (Fig. S8, Fig. S9). While the control and chitosan-coated samples did not exhibit hydrophobic dynamic contact angles and the water droplet was quickly absorbed after being deposited on the sample surface, the UP1 sample proved to have excellent hydrophobicity even during movement. However, the sample was found to be rough by the AFM analysis (Fig. S10), which disabled to perform the tilting contact angle measurements effectively, as the droplet did not roll-off even at the highest tilting angle (88°). The volume-changing method showed a contact angle hysteresis of 5.12° for CO UP1 and 1.54°for PES UP1. The PFAS-coated sample had a lower contact angle hysteresis when applied on CO (4.01°), presumably due to lower surface roughness and a similar value when applied on PES (3.36°). However, as the number of coating layers could improve mechanical properties or durability, therefore they were analyzed subsequently.

The visual appearance of the scaled-up bio-based sample and the PFAS-coated sample was evaluated by measuring the CIE L*a*b* color coordinates (Table S4) and determining the color strength (K/S values) (Fig. 2d). The CIE L*a*b* color measurements indicate that there is only a slight difference between the control and coated CO and PES samples, as the values of all color coordinates (white-black, green-red and blue-yellow) remained on the same side of the color coordinates. The color strength of the samples was determined by the K/S values, where an increased value means that the color of the sample is stronger. The K/S measurements of the CO and PES samples indicate that the values after coating application do not show any significant change compared to the control sample. The CO sample coated with one layer of bio-based coating, shows a similar value of color strength (K/S = 0.0078) as the uncoated CO fabric (K/S = 0.0094). By increasing the number of coatings, the value increases slightly to 0.0109. For the PES sample, the differences are even smaller, and the K/S value remains at a similar level for all samples (0.0430–0.456). Similar K/S values are measured for the PFAS coated samples (K/S = 0.0091 and 0.0467). The results indicate that the color of the samples remains largely unchanged after one, two, or three consecutive applications of the bio-based formulation or the commercial PFAS coating, demonstrating that our developed bio-based coating achieves color properties comparable to those of the commercial baseline. The scanned samples (Fig. S6) show that the color difference is not visible to the naked eye.

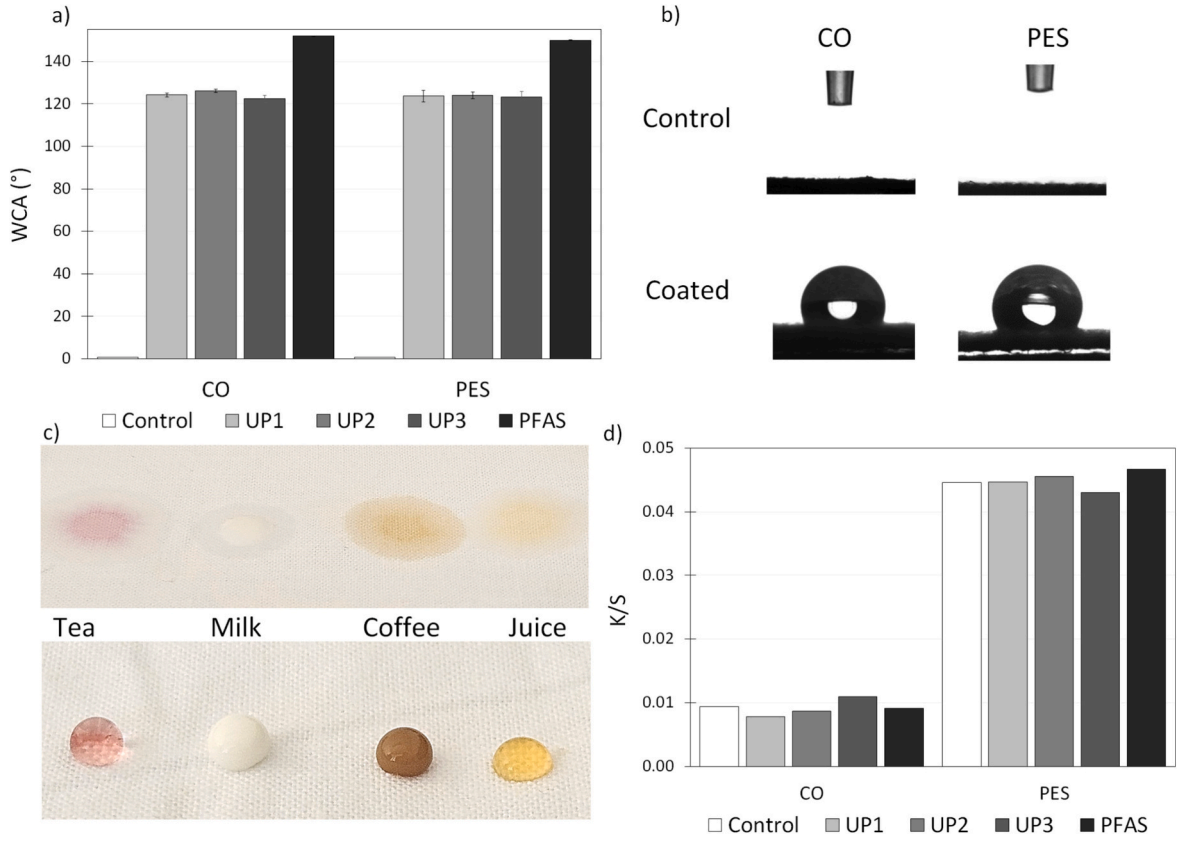

Fig. 2. Demonstration of wettability: a) WCA, b) water droplets, c) coating resistance to droplets of tea, milk, coffee, and juice; d) K/S values of the control, and coated (bio-based and PFAS) CO and PES samples.

2.5. *Morphological and structural properties*

The morphological and elemental characteristics of the scaled-up samples were analyzed to investigate the correlation with the functional performance. Large particles of OSA-modified starch (Lang et al., 2024) are visible in the gaps between the fibers on SEM micrographs particularly of the CO sample (Fig. 3a), which also has a rough, porous, capillary-interconnected coating structure observed at higher magnifications. A similar coating structure was reported by Staneva et al. (2023), where the authors explained that the specific structure was formed due to the modification of chitosan with aldehydes (Staneva et al., 2023). Although still present, a reduced number of OSA-modified starch particles is observed in the PES sample (Fig. 3b), which also exhibits a significantly smoother morphology. In general, it appears that less coating remains on the PES samples, which was confirmed by the smaller increase in mass per unit area compared to CO (Fig. 6). This may be due to the fiber structure itself, as cotton is known for its abundance of hydroxyl groups which are present in smaller amount in polyester, thus affecting its interaction with other materials. The PFAS coated samples (Fig. 3c-d) show a smoother coating surface which is especially visible at higher magnifications. However, the coating appears to have a tendency to form aggregated clumps that bind the individual fibers together. Large patches of PFAS coating can be seen on both the CO and PES samples.

Following the SEM analysis, which provided a detailed imaging of the sample's surface morphology, we proceeded with EDS mapping, to examine the elemental composition of the samples. The bio-based scaled-up sample (UP3) was analyzed for the presence of zinc, while the PFAS benchmark samples were analyzed for fluorine. Analysis of the scaled-up samples containing ZnO, confirmed that the zinc is uniformly distributed over the entire surface of the CO and PES fabrics (Fig. 4a-b), proving the homogeneity of the bio-based scale-up coating and application. In order to determine, whether the coating layers cover and conceal the fiber surface, and to investigate whether the coating penetrates into the interior of the fabric, SEM and EDS analysis of the UP3 CO sample cross section was performed. As it can be seen from the SEM micrograph of the cross section (Fig. 4c), the individual coating layers are not visible. The dip-coating process, in which the entire sample is immersed in the coating dispersion, allows the coating to access the inner layers of the fabric. As the immersion is followed by wringing on the double cylinder foulard, the excess coating is removed, allowing a thin and uniform coating layer to be applied over the entire sample surface. The appropriate application method prevents the coating from completely covering the surface and closing the fabric weave and pores of the fibers to such an extent that a completely sealed, non-permeable coating layer would be formed. Furthermore, the EDS mapping revealed that the zinc (in the form of ZnO) present in the bio-based coating was not only present on the outer layers, but had been absorbed into the interior of the fabric (Fig. 4d), indicating that the coating was uniformly distributed throughout all layers of the fabric. In addition, the concentration of zinc on the surface was determined at three points on the CO and PES scaled-up samples (Fig. 4g). For the CO sample, the zinc concentration increased with the number of coating layers (from 0.29 ± 0.08 to 0.4 ± 0.12 wt%), which correlates well with the 0.1 wt% of ZnO deposition per treatment (ZnO molar mass only 17 % higher than of Zn), while the values for the PES sample were more irregular and did not increase with the number of coating layers (from 0.09 ± 0.04 to 0.18 ± 0.06 wt%). This is consistent with the SEM micrographs (Fig. 3b) and the EDS mapping of zinc (Fig. 4b), where a smaller amount of zinc is visible on the micrograph image compared to the CO sample. The EDS of the PFAS baseline samples showed a significantly greater amount of fluorine present on the CO sample compared to the PES sample, which is consistent with the previous SEM and EDS mapping results.

In order to gain insight into the interaction between the main

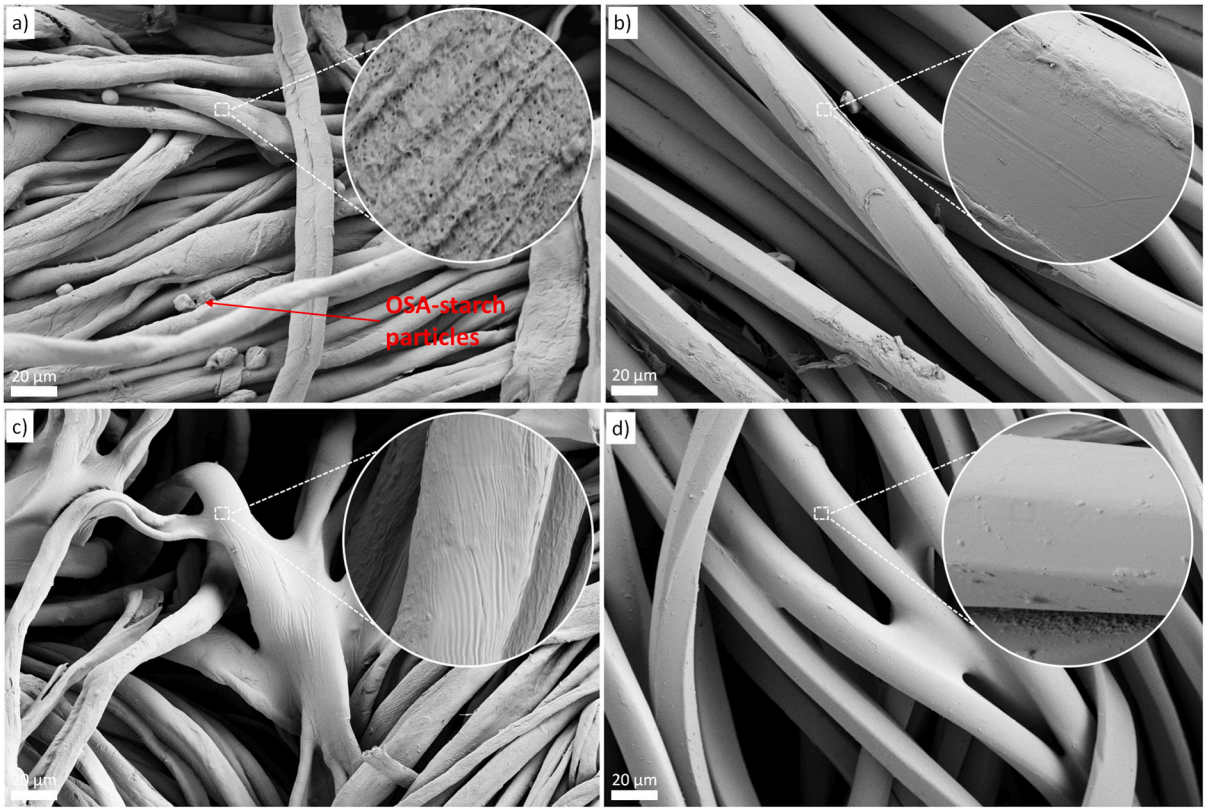

Fig. 3. The SEM micrographs of the bio-based scaled-up (UP3) a) CO and b) PES sample and PFAS coated c) CO and d) PES sample at 1000× and 10,000× magnification.

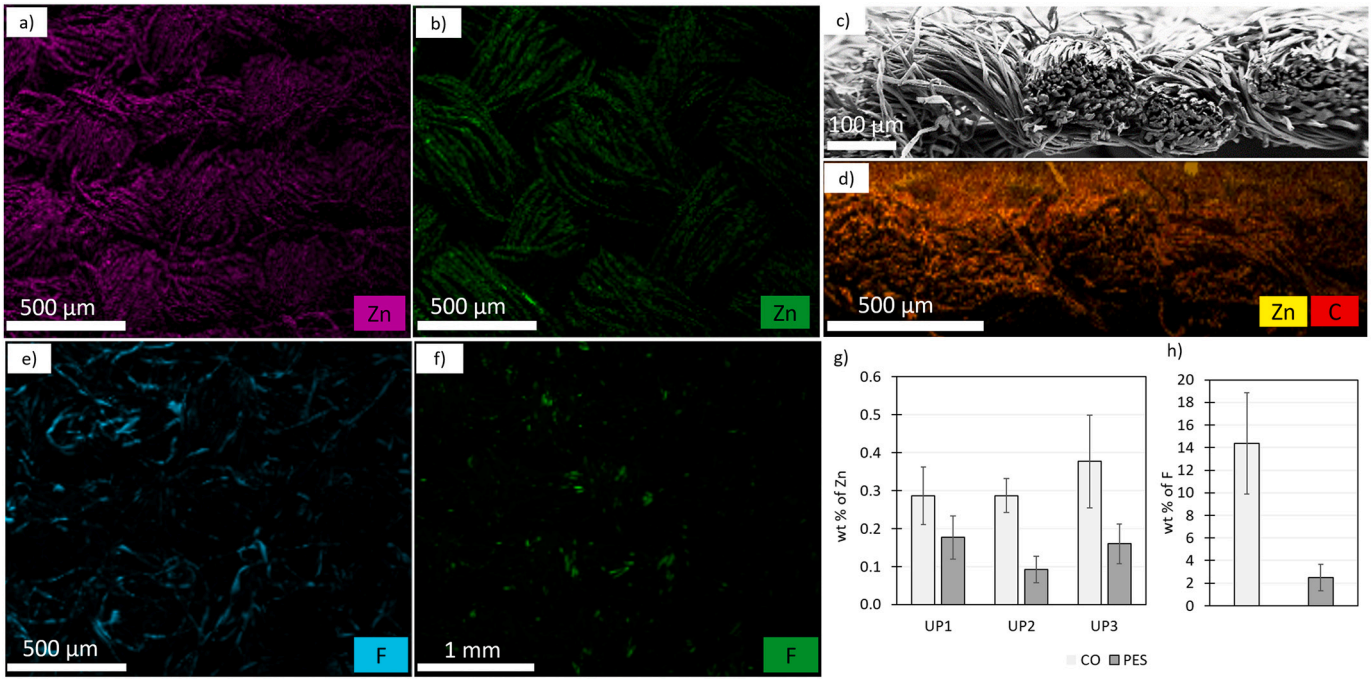

Fig. 4. EDS mapping of zinc on a) CO and b) PES bio-based scaled-up samples, c) SEM and d) EDS mapping of bio-based scaled-up CO sample's cross-section, EDS mapping of fluorine one) CO and f) PES benchmark PFAS sample, and g) wt% of zinc and h) wt% of fluorine on bio-based scaled-up and benchmark PFAS sample.

components of the coating, ATR-FTIR analysis was performed (Fig. 5). Chitosan powder exhibits its characteristic peaks related to OH and NH stretching vibrations between 3700 and 3100 cm^{-1}, CH stretching vibrations between 3050 and 2800 cm^{-1}, amide-I band located at 1730 cm^{-1}, and a peak at 1560 cm^{-1} related to amide-NH_2 absorption band (H. Liu et al., 2013; Oberlintner et al., 2022). In modified starch, OSA—S9, a broad peak related to OH stretching (between 2800 and 3100 cm^{-1}), peaks corresponding to CH stretching vibrations (around

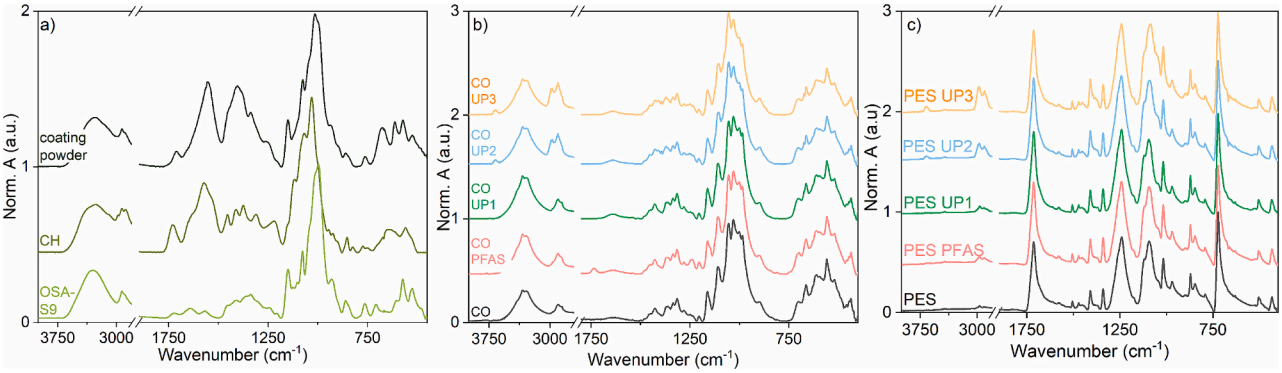

Fig. 5. ATR-FTIR spectra of a) modified starch (OSA—S9), chitosan (CH), and the developed coating consisting of chitosan matrix, modified starch and ZnO particles (CH + OSA-S9 + ZnO); b) uncoated CO (CO), and CO with commercially available PFAS (CO PFAS), and CO coated with the developed bio-based coating (CO UP1, CO UP2, CO UP3); c) uncoated PES (PES), PES coated with PFAS (PES PFAS), and PES coated with the developed coating (PES UP1, PES UP2, PES UP3).

2900 cm^{-1}), peak associated with C═O stretching vibration at 1723 cm^{-1}, and OH bending of water (at 1630 cm^{-1}) were observed (Ren et al., 2017; Xu et al., 2005). Bands at 1152, 1076, 1000, and 933 cm^{-1} are related to C—O, C—O—H and C—O stretching in the biopolymer backbone (Li et al., 2021). When forming a complex between the two components, peaks in this region (between 1200 and 900 cm^{-1}), which is typical of polysaccharides are slightly shifted to higher frequencies, suggesting interactions between the chains. Additionally, indicative of the interactions between the amino groups of chitosan and the hydroxyl groups of starch, the amide-I and N—H peaks in chitosan shifted to 1709 cm and 1555 cm^{-1}, respectively, demonstrating improved compatibility between the two biopolymers (Ren et al., 2017). Possible structural changes, which would also indicate changes in the properties of CO and PES surfaces upon coating with PFAS and chitosan-based coatings were investigated. When both CO and PES were coated with the developed bio-based coating, the spectra closely resembled the ones of uncoated textiles, however with enhanced CH-related vibrations at 2900 cm^{-1}, which became even more prominent with increasing the number of layers applied, indicating the presence of the coating (Fig. 5b and c). The PFAS-coated CO fabric revealed newly emerged peak at 1736 cm^{-1}, associated with C═O bonds that are present in PFAS (Fig. S7), confirming the deposition of the coating onto the surface.

2.6. Functionality, durability and stability of the coated textiles

Commercial PFAS coatings are well-known for their longevity, particularly when it comes to resistance against washing and wearing. To evaluate how our bio-based coatings compare in performance to the benchmarks set by PFAS coatings, we analyzed the sample's mechanical properties, durability to washing, abrasion resistance and the effect of sample aging on WCA.

The physical properties of textiles play a crucial role in determining their functionality and use in real-world applications. The application of coatings can significantly alter properties, such as bending rigidity, grammage and thickness, impacting how they look and feel. The fabric mass per unit area (the grammage) (Fig. 6a) of the bio-based scaled-up samples increased slightly as the number of coating layers increased. The PFAS coated samples, which were coated with a single layer of coating, have similar to slightly increased values compared to the bio-based samples. The greatest differences are observed in the inherent properties of the different fabrics themselves. Similarly, the thickness of the bio-based CO samples also slightly increases with the number of coating layers (Fig. 6a). The bio-based PES samples maintain similar thickness values among all three samples, while the PFAS-coated PES sample reaches a similar thickness as the uncoated (control) sample. The

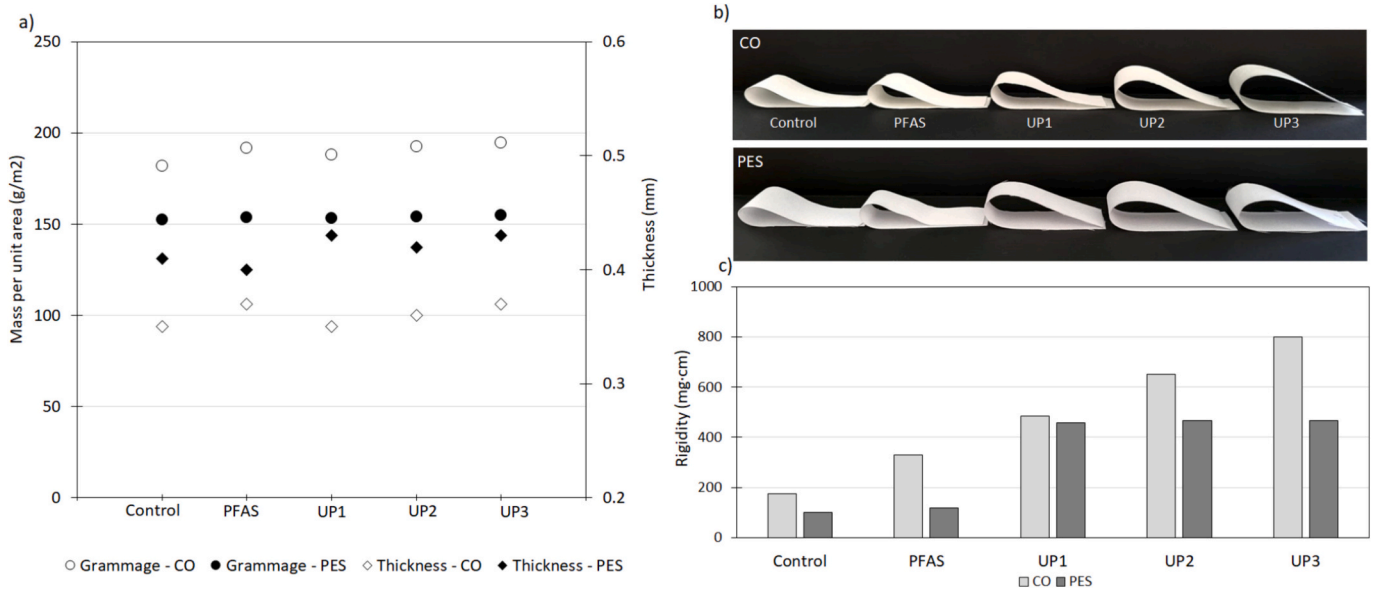

Fig. 6. a) Mass per unit area (g/m^2), thickness (mm), b) images presenting the stiffness of the samples and c) overall rigidity of the control, PFAS, UP1, UP2, UP3 coated CO and PES samples.

differences between all the measurements are minimal and fall within a range that is unlikely to be noticeable under typical real-world conditions.

The stiffness of the control and coated samples was assessed by measuring the rigidity (Fig. 6b, c). The control CO and PES samples are soft and flexible with overall rigidity values of 176.15 mg·cm (CO) and 100.05 mg·cm (PES). Application of either the bio-based or PFAS coating resulted in increased rigidity, which is more pronounced for the CO samples. By applying PFAS coating, the stiffness of the CO increased to 329.82 mg·cm and to 117.27 mg·cm for PES. By applying one layer of bio-based coating (UP1), the values increase to 485.46 mg·cm for CO and 457.00 mg·cm for PES. The values increase further by applying two (UP2) or three (UP3) layers of coating, however, a much larger increase is observed for the CO samples. This is in good agreement with the SEM results (Fig. 3), EDS results (Fig. 4) and the mass per unit area results (Fig. 6a). The rigidity of the bio-based coated PES samples increases only slightly with additional layer application. This can be well observed from the image of the coated samples (Fig. 6b), where the stiffness of the CO UP1, UP2 and UP3 samples slightly increases with increasing the number of layers, while the PES stiffness remains similar regardless of the number of coating layers. While numerically, the rigidity values increase significantly with the application of all coatings, in real life the values are not high enough that the rigidity would significantly affect the hand-feel and usability of the fabric. The literature on coated textiles shows similar or higher rigidity values, with the increased rigidity of up to 700 to 1800 % for the samples coated with hydrophobic coating compared to the uncoated samples (Dignes et al., 2024; Golja et al., 2013; Simončič et al., 2014).

Among the mechanical properties of the textiles, we focused on the breaking strength and elongation at break of the control, bio-based scaled-up and PFAS coated samples (Fig. 7a and b) in both warp and weft directions. The results showed minimal differences in the force required to break the CO samples, whether uncoated or coated. This suggests that the coatings did not significantly alter the mechanical strength of the fabrics, as the primary load-bearing components are the fibers themselves and not the applied coating. This also confirms that the application of the developed coating, did not compromise the mechanical integrity of the fabric, and that the fibers were not chemically or physically damaged during the coating process. The greatest difference observed was noticed between the values of the CO and PES fabrics in general, which is primarily due to the inherent properties of the material itself. However, the force required to break the PES sample in the warp direction increases in the following order: control, UP1, UP2, UP3, PFAS, indicating that the number of coating layers increases the force required to break the sample, which could be due to the increased thickness and mass per unit area of the samples achieved by applying multiple coating layers (Fig. 6). At the same time, the control PES sample has a much higher standard deviation between the breaking strength measurements, than the bio-based scaled-up or PFAS coated PES samples. The difference in material properties is also observed when measuring elongation at break, where again higher values are observed for the PES samples. A slight increase in values was observed for the PFAS-coated PES sample in both the warp and weft directions, indicating that the PFAS coating may affect the elongation at break of the PES fabric. In contrast, the PFAS-coated CO sample exhibited values similar to those of the bio-based coated samples. Despite the changes

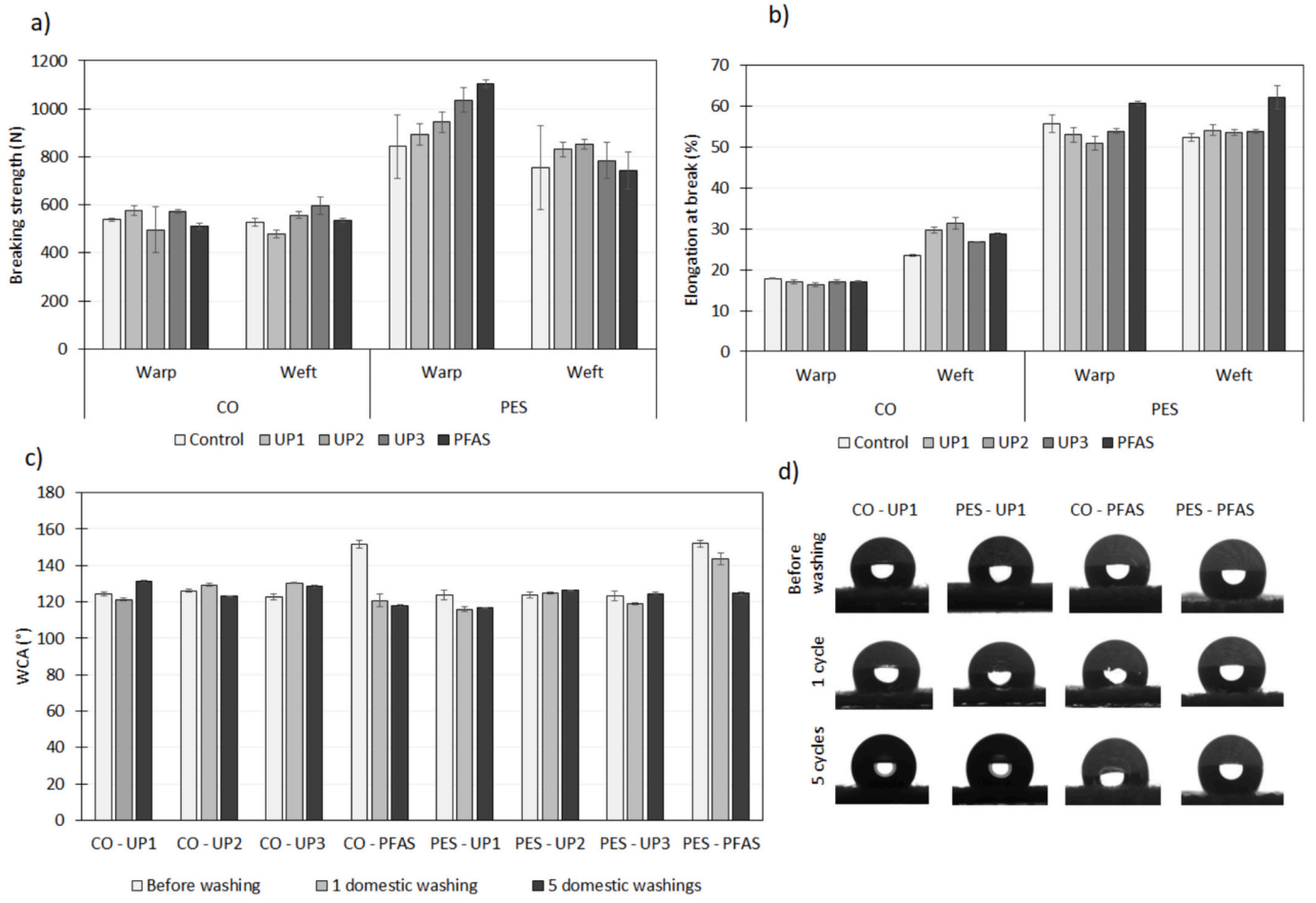

Fig. 7. Mechanical properties of bio-based and PFAS coated samples: a) Breaking strength, b) elongation at break, c) WCA before and after 1 and 5 domestic washing cycles and d) images of measured WCA for bio-based scaled-up and PFAS coated samples.

observed, no clear correlation could be established between the number of coating layers and the measured strength or elongation values, expected in either the warp and weft direction or in both materials, suggesting that the number of layers applied does not directly influence the mechanical behavior in a predictable manner. The elongation and strength values remained comparable, indicating that the newly developed coatings performed similarly to commercial benchmark coatings.

The washing durability of the samples was evaluated by performing a laboratory simulation of one and five domestic washings (Fig. 7d). The control CO and PES samples are so hydrophilic that it is not possible to measure their WCA, therefore their measurements are given as <10°. The WCA of the control samples remains immeasurably low after 1 or 5 washing cycles. The measurements of the washed bio-based scaled-up samples indicate that the WCA values do not decrease notably after 5 domestic washing cycles. In some cases, the values even slightly increased, which could be due to the chemical or weave structure changes during the washing. This suggests that the coating effectively retains its hydrophobic properties even after repeated washing. No significant correlation can be established between the number of coating layers and the measured WCA values after washing, suggesting that increasing the number of coating layers (UP1, UP2, UP3) does not provide prolonged washing durability of the coating. While the PFAS-coated samples initially exhibit excellent water repellency, the WCA values show a significant decrease after the first washing cycle, with further decreases observed after five domestic washing cycles, bringing their WCA close to that of the bio-based scaled-up samples.

The abrasion resistance of the bio-based and PFAS-coated samples was evaluated by performing the Martindale abrasion test (Fig. 8a). The WCA of the bio-based scaled-up CO samples decreased with increasing number of abrasion cycles, however, the values still remained high enough to be hydrophobic even after 20,000 cycles, while the PFAS sample shifts to hydrophilic after only 5000 rub cycles, indicating a susceptibility to wear and loss of protective properties. In addition, the CO samples retained their hydrophobic properties regardless of the number of coating layers applied. The bio-based CO sample has performed significantly better than the baseline PFAS coating on CO, demonstrating an important advantage of the novel coating developed in frame of this research. The improved performance of the bio-based coating compared to the commercial PFAS coating may be due to its superior homogeneity, as confirmed by SEM and EDS analyses. This behavior is not observed when focusing on PES samples. Both the bio-based and PFAS-coated PES samples effectively maintain their hydrophobic properties throughout the rubbing cycles. Similar to the CO bio-based samples, no significant differences in coating durability are

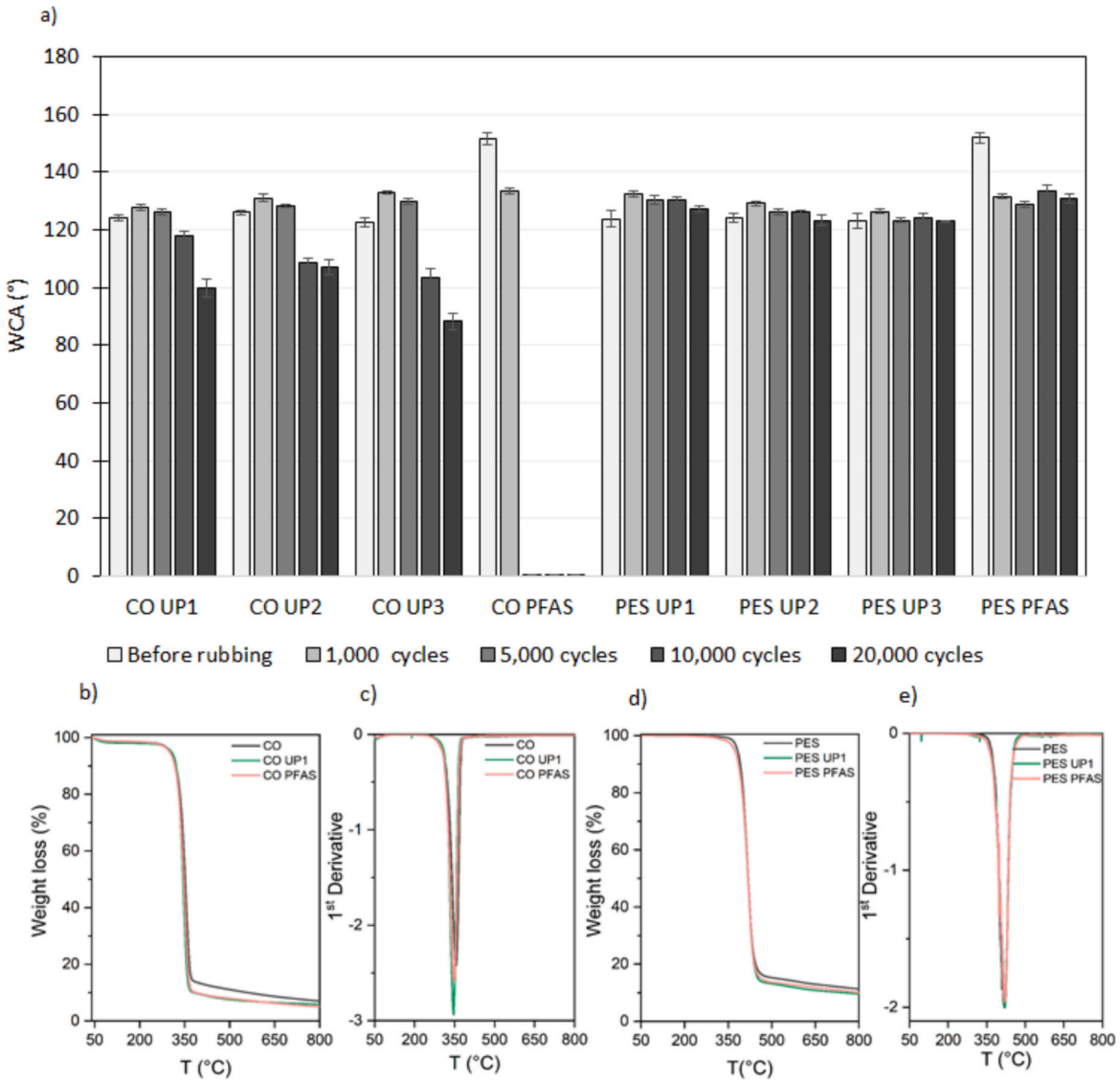

Fig. 8. a) Abrasion resistance of CO and PES samples over 20,000 rubbing cycles, b) thermal stability of bio-based and PFAS coated of CO and PES samples.

observed in relation to the number of coating layers applied. However, a substantial difference in the stability of the PFAS coating on PES compared to CO is evident. The WCA shows a decrease after the initial 1000 abrasion cycles, while WCA of the sample remains stable thereafter. The difference in durability could be attributed to the chemical structure of the materials and their ability to bind with the compounds from the coatings, affecting their stability.

The thermal stability of the samples was evaluated through TGA. Since the number of coated layers did not show any effect on the thermal stability, only UP1 from the scaled-up samples are presented for clarity (Fig. 8b-e), while UP2 and UP3 can be found in the Supplementary information (Fig. S11). Focusing first on CO, both uncoated and coated with UP1 and PFAS exhibit the same trend. The decomposition occurs in two phases: i) water loss up to temperatures of 105 °C (up to 2 wt%), and ii) main decomposition phase with a starting temperature of 215 °C. The temperature of maximum weight loss differs slightly between the samples, with uncoated CO having the highest (354 °C) followed by PFAS coated (347 °C) and bio-based coating (346 °C). Since the coating represents around 3 wt% of the sample, the difference can be attributed to the fact that the temperature of the maximum degradation of bio-based coating is 295 °C (Fig. S11). For similar reasons, the char residue of CO UP1 and PFAS (6 and 5 wt%, respectively), is slightly lower than that of the uncoated sample (7 wt%). On the other hand, PES, coated or uncoated, does not exhibit any water loss and decomposes in only one phase starting at 285 °C. Maximal degradation for all three samples (PES, PES UP1 and PES PFAS) is at 421 °C. Again, the char residue is 1 wt % higher in the uncoated samples compared to the coated one (10 wt%), contributing to the weight of the coating. Based on these findings, the coating shows sufficient thermal stability of CO and PES fabrics, comparable to commercially available fluorine-based coatings.

The long-term stability of the samples was evaluated by monitoring the aging of the samples and its effect on the hydrophobicity of the samples. The WCA of the bio-based scaled-up samples was measured the day after preparation, after 40 days, and after 80 days to assess any changes in hydrophobicity over time (Fig. 9a). The results showed that all CO samples showed an increase in WCA 40 days after preparation, but with a large standard deviation between measurements. The PES samples showed a decrease in WCA over the same time period. However, the measurements taken 80 days after production show a decrease compared to the values recorded at 40 days. Nevertheless, these values remain approximately the same or higher than those measured on the day of production for the CO samples. At the same time, the values show a similar or smaller standard deviation than the values measured on the day of production of 40 days, suggesting that as the samples age, their surfaces become more uniform, resulting in less variability in the measured values and more homogeneous and consistent surface properties, regardless of the number of coating layers. The PES samples showed a slight decrease in WCA after 40 and 80 days compared to the day after sample preparation, but their hydrophobicity was maintained. To further evaluate the sustained hydrophobic performance of the coated samples beyond the initial 80-day period, additional measurements were taken after 230 days. The WCA of the CO and PES samples remained stable, with no significant decrease in WCA values observed. All samples exhibited WCA values similar to those measured at 80 days, with a few degrees of fluctuation in increase or decrease. The results indicate that the bio-based scale-up samples effectively retained their hydrophobic properties making them stable over prolonged periods of time. In addition to long-term stability, biodegradability in soil tests were performed on the standalone coating material. The results demonstrated that the biopolymer component of the coating decomposes rapidly under soil conditions (Fig. S14), highlighting its environmental compatibility, alongide the functional stability when applied on the textile material.

In addition, water absorption was monitored by exposing the samples to water droplets for 5 min (Fig. 9b). The results showed that all samples effectively retained their hydrophobic properties for the first 60 s of exposure. Furthermore, the CO samples effectively maintained their level of hydrophobicity throughout the 5 min period, regardless of the number of coating layers. Although a slight difference in the measured WCA was observed when comparing the number of coating layers - the highest WCA was measured for the UP2 sample, followed by the UP1 sample. The PES samples showed significantly different results. While all three samples maintained their WCA for the first 60 s, the WCA values of the UP1 and UP2 samples decreased significantly thereafter, suggesting that the number of coating layers may have an effect on the hydrophobicity of PES fabrics during prolonged exposure to water. These results further emphasize the importance of evaluating the aging, prolonged water exposure and number of coating layers to better

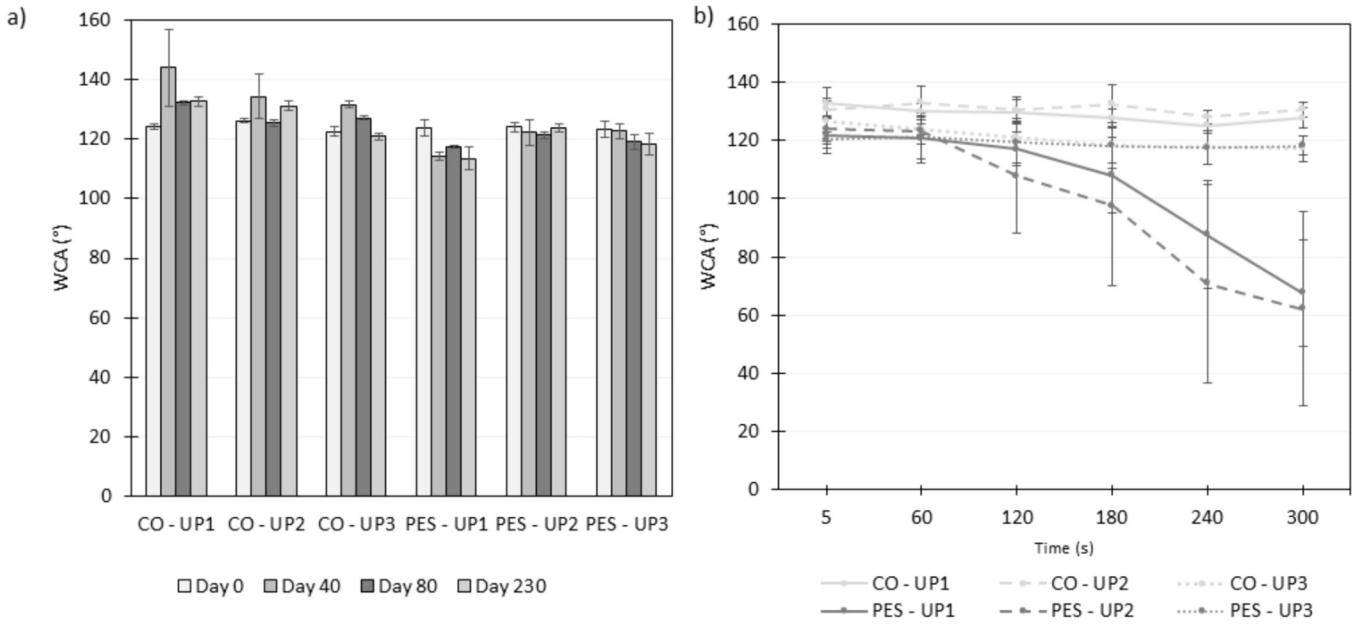

Fig. 9. a) WCA measurements of the samples UP1, UP2 and UP3 CO and PES samples the day after production, after 40 days, after 80 days and after 230 days, and b) WCA of the 80-days old bio-based scaled-up samples through five-minute timeframe.

understand the durability and stability of the developed coating in real-world applications.

2.7. Multivariate statistical analysis

The effects of multiple consecutive coatings of the bio-based formulation on the sample's properties and durability were further investigated by performing a multivariate statistical analysis, aiming to determine whether there is a significant benefit to using multiple layers of coating to achieve the desired properties, or if a single layer would be sufficient. The results show two major clusters that are separated by high bootstrap values ($n = 100$), indicating that the overall multivariate characteristics of the coated and the control fabric (either CO or PES) are significantly different (Fig. 10). This shows the influence of the coating itself, irrespective of its nature, the number of coating layers (n = 1, 2 or 3) or the underlying material. Also, the surface characteristics of the uncoated materials are rather similar, as they are grouped together on the same branch. The PFAS-coated fabrics were tightly grouped in close proximity to multiple bio-based coating layers of the same fabric showcasing that the developed coatings exhibit highly similar characteristics to the commercial PFAS coating utilized on the same fabric in the same experiments according to the parameters measured in this study (resistance to washing, mechanical properties, abrasion resistance, aging of the sample, water absorption, TGA). Although somewhat surprising, the number of coats exhibited rather minimal influence on the measured surface characteristics as they were all grouped on the same branch with respect to the underlying CO or PES fabric. The smallest differences were observed between the number of coats. Single and double coating layer on polyester exhibited somewhat more similar surface characteristics and differed from the triple coating layers of polyester fabric, whereas for cotton, the main difference was between the first and all consecutive coating layers (double and triple coats). Overall, the results clearly show that irrespective of the differences in the number of coating layers, the overall properties of the developed coatings are highly similar to the commercially available PFAS coating utilized in this study. Even more, the approach developed here enables us to perform multivariate analyses of the coatings therefore utilizing all available information derived from various laboratory tests. The developed analytical and statistical platform enables us to perform analyses in a systematic and compatible ways for achieving the technical requirements, thus supporting the decision making of the industrial partners.

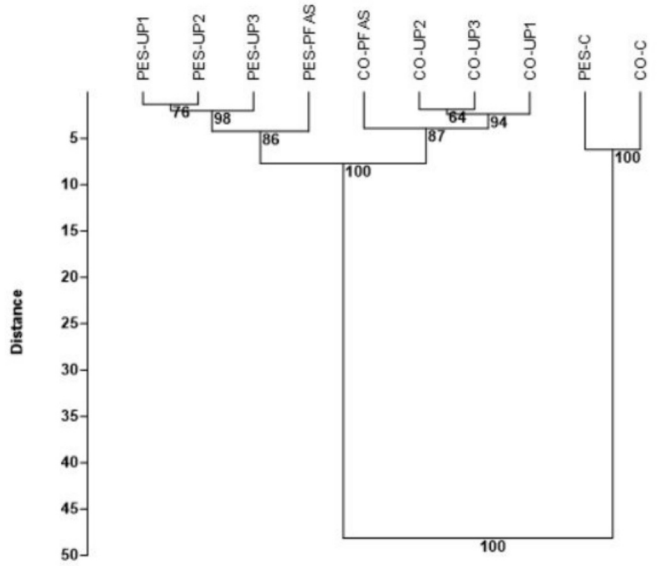

Fig. 10. The figure shows schematic branching of the surface characteristics of CO and PES fabric covered with single (CO_UP1; PES_UP1), double (CO_UP2; PES_UP2) or triple coating layers (CO_UP3; PES_UP3), relative to PFAS coated fabric (CO_PFAS; PES_PFAS) and uncoated controls (CO-C; PES—C). Note the general similarity between the surface characteristics within each final fabric branch (CO or PES) relative to uncoated controls.

3. Conclusions

The present study represents a crucial step towards mitigating the environmental and health risks associated with PFAS, by introducing a novel, easily scalable solution for hydrophobizing textiles, using renewable and biodegradable biopolymers. Given the urgent need to phase out PFAS due to their persistent environmental pollution and health impacts, in frame of this paper, the application of the developed bio-based hydrophobic coating was scaled-up from laboratory scale to pilot scale, demonstrating its practical viability for commercial use. The coating based on chitosan, OSA-modified starch and ZnO nanoparticles provides hydrophobicity with WCA's up to 132° on cotton and 126° on polyester, while not noticeably affecting the hand feel and stiffness of the samples. Notably, this bio-based coating outperformed the commercial fluorine-containing coatings in terms of abrasion resistance, while maintaining mechanical strength and stability after washing comparable to PFAS-coated samples. Additionally, the water-repellent properties remained stable for at least 230 days, thereby reducing the need for frequent reapplication. The biodegradation analysis of the coating formulation proved that the biopolymer component of the film fully degraded in 8 days, while inorganic residue remained present. The multivariate statistical analysis showed that the developed bio-based coatings exhibited highly similar properties to the commercially available PFAS coating. At the same time, there was no significant difference between 1, 2 and 3 layers of bio-based coating on textiles, suggesting that increased number of coating layers did not significantly contribute to better functional properties. Overall, the study represents a significant advancement in the field of sustainable textile coatings, providing a starting point and encouraging further exploration of bio-based materials for coatings in the textile industry.

Supplementary data to this article can be found online at https://doi.org/10.1016/j.carbpol.2025.123792.

CRediT authorship contribution statement

Anja Verbič: Writing – review & editing, Writing – original draft, Visualization, Methodology, Investigation, Formal analysis, Data curation, Conceptualization. **Blaž Stres:** Writing – review & editing, Writing – original draft, Supervision, Investigation, Data curation. **Ivan Jerman:** Methodology, Investigation. **Barbara Golja:** Methodology, Investigation, Formal analysis. **Ema Žagar:** Investigation, Formal analysis, Data curation. **Vuk Martinović:** Methodology, Investigation, Formal analysis. **Petja Logar:** Methodology, Investigation, Formal analysis. **Gregor Lavrič:** Writing – review & editing, Writing – original draft, Methodology, Investigation, Formal analysis. **Anže Prašnikar:** Writing – review & editing, Writing – original draft, Investigation, Formal analysis. **Blaž Likozar:** Supervision, Resources, Project administration, Funding acquisition. **Uroš Novak:** Project administration, Funding acquisition, Conceptualization. **Ana Oberlintner:** Writing – review & editing, Writing – original draft, Validation, Supervision, Methodology, Investigation, Formal analysis, Data curation, Conceptualization.

Funding

This research was supported by Horizon Europe project PROPLANET (Grant agreement number 10109842) and Slovenian Research and Innovation Agency (Research core funding No. P2–0152 and project J4–50148).

Declaration of competing interest

The authors declare that they have no known competing financial interests or personal relationships that could have appeared to influence the work reported in this paper.

Acknowledgements

The authors would like to thank Andrej Race and Nigel Van de Velde for the help with AFM analysis.

Data availability

Data will be made available on request.

References

Ackerman Grunfeld, D., Gilbert, D., Hou, J., Jones, A. M., Lee, M. J., Kibbey, T. C. G., & O'Carroll, D. M. (2024). Underestimated burden of per- and polyfluoroalkyl substances in global surface waters and groundwaters. *Nature Geoscience, 17*(4), 340–346. https://doi.org/10.1038/s41561-024-01402-8

Altuna, L., Herrera, M. L., & Foresti, M. L. (2018). Synthesis and characterization of octenyl succinic anhydride modified starches for food applications. A review of recent literature. *Food Hydrocolloids, 80*, 97–110. https://doi.org/10.1016/j.foodhyd.2018.01.032

Bai, Y., & Shi, Y.-C. (2011). Structure and preparation of octenyl succinic esters of granular starch, microporous starch and soluble maltodextrin. *Carbohydrate Polymers, 83*(2), 520–527. https://doi.org/10.1016/j.carbpol.2010.08.012

Bajić, M., Jalšovec, H., Travan, A., Novak, U., & Likozar, B. (2019). Chitosan-based films with incorporated supercritical CO2 hop extract: Structural, physicochemical, and antibacterial properties. *Carbohydrate Polymers, 219*, 261–268. https://doi.org/10.1016/j.carbpol.2019.05.003

Bartell, S. M., & Vieira, V. M. (2021). Critical review on PFOA, kidney cancer, and testicular cancer. *Journal of the Air & Waste Management Association, 71*(6), 663–679. https://doi.org/10.1080/10962247.2021.1909668

Barthlott, W., & Neinhuis, C. (1997). Purity of the sacred lotus, or escape from contamination in biological surfaces. *Planta, 202*(1), 1–8. https://doi.org/10.1007/s004250050096

Bashari, A., Salehi, K., H, A., & Salamatipour, N. (2020). Bioinspired and green water repellent finishing of textiles using carnauba wax and layer-by-layer technique. *The Journal of the Textile Institute, 111*(8), 1148–1158. https://doi.org/10.1080/00405000.2019.1686881

Blake, B. E., Pinney, S. M., Hines, E. P., Fenton, S. E., & Ferguson, K. K. (2018). Associations between longitudinal serum perfluoroalkyl substance (PFAS) levels and measures of thyroid hormone, kidney function, and body mass index in the Fernald community cohort. *Environmental Pollution, 242*, 894–904. https://doi.org/10.1016/j.envpol.2018.07.042

Byun, D., Hong, J., Saputra, K., J. H., L., Lee, Y. J., Park, H. C., … Lukes, J. R. (2009). Wetting characteristics of insect wing surfaces. *Journal of Bionic Engineering, 6*(1), 63–70. https://doi.org/10.1016/S1672-6529(08)60092-X

Cheng, Q.-Y., Guan, C.-S., Wang, M., Li, Y.-D., & Zeng, J.-B. (2018). Cellulose nanocrystal coated cotton fabric with superhydrophobicity for efficient oil/water separation. *Carbohydrate Polymers, 199*, 390–396. https://doi.org/10.1016/j.carbpol.2018.07.046

CompTox. (2022a). EPA PFAS chemicals without explicit structures. https://comptox.epa.gov/dashboard/chemical-lists/PFASDEV.

CompTox. (2022b). PFAS structure list. https://comptox.epa.gov/dashboard/chemical-lists/PFASSTRUCT.

Cunha, A. G., & Gandini, A. (2010). Turning polysaccharides into hydrophobic materials: A critical review. Part 1. cellulose. *Cellulose, 17*(5), 875–889. https://doi.org/10.1007/s10570-010-9434-6

Dai, M., Zhai, Y., & Zhang, Y. (2021). A green approach to preparing hydrophobic, electrically conductive textiles based on waterborne polyurethane for electromagnetic interference shielding with low reflectivity. *Chemical Engineering Journal, 421*, Article 127749. https://doi.org/10.1016/j.cej.2020.127749

De Berardis, B., Civitelli, G., Condello, M., Lista, P., Pozzi, R., Arancia, G., & Meschini, S. (2010). Exposure to ZnO nanoparticles induces oxidative stress and cytotoxicity in human colon carcinoma cells. *Toxicology and Applied Pharmacology, 246*(3), 116–127. https://doi.org/10.1016/j.taap.2010.04.012

Department of Environmental Conservation. (2025). PFAS in apparel law. https://dec.ny.gov/environmental-protection/help-for-businesses/pfas-in-apparel-law.

Dignes, C., Nicolas, N. J., Schroeder, T. B. H., & Aizenberg, J. (2024). Robust PFAS-free superhydrophobicity exhibited in hierarchically nanostructured coatings on textiles. *Advanced Engineering Materials*, Article 2401736.

ECHA. (2023). ECHA publishes PFAS restriction proposal. https://echa.europa.eu/sv/-/echa-publishes-pfas-restriction-proposal.

Fan, C., Zhang, M., Hou, Y., Wang, X., Xia, S., & Fang, Z. (2025). Effects of molecular weight of chitosan on its binding ability with OSA starch and oil-water interface behavior of complex-stabilized emulsion. *International Journal of Biological Macromolecules, 292*, Article 139226. https://doi.org/10.1016/j.ijbiomac.2024.139226

FDA. (2025, February 13). SCOGS (Select Committee on GRAS Substances) https://www.hfpappexternal.fda.gov/scripts/fdcc/index.cfm?order=ASC&set=SCOGS&showAll=true&sort=Sortsubstance&type=basic&utm_source=chatgpt.com.

FDA. (2025, February). 13. Substances Added to Food https://www.hfpappexternal.fda.gov/scripts/fdcc/index.cfm?set=FoodSubstances&sort=Sortterm_ID&order=ASC&showAll=true&type=basic&search.

Fenton, S. E., Ducatman, A., Boobis, A., DeWitt, J. C., Lau, C., Ng, C., … Roberts, S. M. (2021). Per- and Polyfluoroalkyl substance toxicity and human health review: Current state of knowledge and strategies for informing future research. *Environmental Toxicology and Chemistry, 40*(3), 606–630. https://doi.org/10.1002/etc.4890

Forsman, N., Johansson, L.-S., Koivula, H., Tuure, M., Kääriäinen, P., & Österberg, M. (2020). Open coating with natural wax particles enables scalable, non-toxic hydrophobation of cellulose-based textiles. *Carbohydrate Polymers, 227*, Article 115363. https://doi.org/10.1016/j.carbpol.2019.115363

Forsman, N., Lozhechnikova, A., Khakalo, A., Johansson, L.-S., Vartiainen, J., & Österberg, M. (2017). Layer-by-layer assembled hydrophobic coatings for cellulose nanofibril films and textiles, made of polylysine and natural wax particles. *Carbohydrate Polymers, 173*, 392–402. https://doi.org/10.1016/j.carbpol.2017.06.007

Ghasemi, N., Seyfi, J., & Asadollahzadeh, M. J. (2018). Imparting superhydrophobic and antibacterial properties onto the cotton fabrics: Synergistic effect of zinc oxide nanoparticles and octadecanethiol. *Cellulose, 25*(7), 4211–4222. https://doi.org/10.1007/s10570-018-1837-9

Glüge, J., Scheringer, M., Cousins, T., & I., C. DeWitt, J., Goldenman, G., Herzke, D., Lohmann, R., A. Ng, C., Trier, X., & Wang, Z.. (2020). An overview of the uses of per- and polyfluoroalkyl substances (PFAS). *Environmental Science: Processes & Impacts, 22*(12), 2345–2373. https://doi.org/10.1039/D0EM00291G

Golja, B., Šumiga, B., & Tavčer, P. F. (2013). Fragrant finishing of cotton with microcapsules: Comparison between printing and impregnation. *Coloration Technology, 129*(5), 338–346.

Gonçalves, J., Torres, N., Silva, S., Gonçalves, F., Noro, J., Cavaco-Paulo, A., Ribeiro, A., & Silva, C. (2020). Zein impart hydrophobic and antimicrobial properties to cotton textiles. *Reactive and Functional Polymers, 154*, Article 104664. https://doi.org/10.1016/j.reactfunctpolym.2020.104664

Hahn, T., Bossog, L., Hager, T., Wunderlich, W., Breier, R., Stegmaier, T., & Zibek, S. (2019). Chitosan application in textile processing and fabric coating. In *Chitin and chitosan* (pp. 395–428). In John Wiley & Sons, Ltd.. https://doi.org/10.1002/9781119450467.ch16

Hammer, O., Harper, D. A. T., & Ryan, P. D. (2001). PAST: Paleontological statistics software package for education and data analysis. *Palaeontologia Electronica, 4*(1). https://palaeo-electronica.org/2001_1/past/past.pdf.

Høisæter, Å., & Breedveld, G. D. (2022). Leaching potential of per- and polyfluoroalkyl substances from source zones with historic contamination of aqueous film forming foam—A surfactant mixture problem. *Environmental Advances, 8*, Article 100222. https://doi.org/10.1016/j.envadv.2022.100222

Ivanova, N. A., & Philipchenko, A. B. (2012). Superhydrophobic chitosan-based coatings for textile processing. *Applied Surface Science, 263*, 783–787. https://doi.org/10.1016/j.apsusc.2012.09.173

Kaya, H., Aydın, F., Gürkan, M., Yılmaz, S., Ates, M., Demir, V., & Arslan, Z. (2016). A comparative toxicity study between small and large size zinc oxide nanoparticles in tilapia (Oreochromis niloticus): Organ pathologies, osmoregulatory responses and immunological parameters. *Chemosphere, 144*, 571–582. https://doi.org/10.1016/j.chemosphere.2015.09.024

Kim, S. H., Bae, S., Sung, Y. W., & Hwang, Y. S. (2024). Effects of particle size on toxicity, bioaccumulation, and translocation of zinc oxide nanoparticles to bok choy (Brassica chinensis L.) in garden soil. *Ecotoxicology and Environmental Safety, 280*, Article 116519. https://doi.org/10.1016/j.ecoenv.2024.116519

Land, M. F., & Nilsson, D.-E. (2012). *Animal eyes*. OUP Oxford.

Lang, S., Sui, C., & Wang, L. (2024). Jet milling-activated direct synthesis of octenyl succinic anhydride modified starch: An analysis of structural and application properties. *International Journal of Food Science & Technology, 59*(8), 5490–5501. https://doi.org/10.1111/ijfs.17268

Lavrič, G., Oberlintner, A., Filipova, I., Novak, U., Likozar, B., & Vrabič-Brodnjak, U. (2021). Functional Nanocellulose, alginate and chitosan nanocomposites designed as active film packaging materials. *Polymers, 13*(15), 2523. https://doi.org/10.3390/polym13152523

Li, W., Yu, Y., Peng, J., Dai, Z., Wu, J., & Wang, Z. (2021). Effects of the degree of substitution of OSA on the properties of starch microparticle-stabilized emulsions. *Carbohydrate Polymers, 255*, Article 117546. https://doi.org/10.1016/j.carbpol.2020.117546

Lin, Z., Cheng, H., He, K., McClements, D. J., Jin, Z., Xu, Z., … Chen, L. (2024). Recent progress in the hydrophobic modification of starch-based films. *Food Hydrocolloids, 151*, Article 109860. https://doi.org/10.1016/j.foodhyd.2024.109860

Liu, B.-Y., Xue, C.-H., An, Q.-F., Jia, S.-T., & Xu, M.-M. (2019). Fabrication of superhydrophobic coatings with edible materials for super-repelling non-Newtonian liquid foods. *Chemical Engineering Journal, 371*, 833–841. https://doi.org/10.1016/j.cej.2019.03.222

Liu, H., Adhikari, R., Guo, Q., & Adhikari, B. (2013). Preparation and characterization of glycerol plasticized (high-amylose) starch–chitosan films. *Journal of Food Engineering, 116*(2), 588–597. https://doi.org/10.1016/j.jfoodeng.2012.12.037

Lu, R., Yu, Y., Adkhamjon, G., Gong, W., Sun, X., & Liu, L. (2020). Bio-inspired cotton fabric with superhydrophobicity for high-efficiency self-cleaning and oil/water separation. *Cellulose, 27*(12), 7283–7296. https://doi.org/10.1007/s10570-020-03281-9

Mitjans, M., Marics, L., Bilbao, M., Maddaleno, A. S., Piñero, J. J., & Vinardell, M. P. (2023). Size matters? A comprehensive in vitro study of the impact of particle size on the toxicity of ZnO. *Nanomaterials, 13*(11). https://doi.org/10.3390/nano13111800

Mullangi, D., Shalini, S., Nandi, S., Choksi, B., & Vaidhyanathan, R. (2017). Super-hydrophobic covalent organic frameworks for chemical resistant coatings and hydrophobic paper and textile composites. *Journal of Materials Chemistry A, 5*(18), 8376–8384. https://doi.org/10.1039/C7TA01302G

Oberlintner, A., Likozar, B., & Novak, U. (2021). Hydrophobic functionalization reactions of structured cellulose nanomaterials: Mechanisms, kinetics and in silico multi-scale models. *Carbohydrate Polymers, 259*, Article 117742. https://doi.org/10.1016/j.carbpol.2021.117742

Oberlintner, A., Shvalya, V., Santhosh, N. M., Košiček, M., Jerman, I., Huš, M., … Likozar, B. (2024). Janus nanocellulose membrane by nitrogen plasma: Hydrophilicity to hydrophobicity selective switch. *Carbohydrate Polymers, 345*, Article 122558. https://doi.org/10.1016/j.carbpol.2024.122558

Oberlintner, A., Vesel, A., Naumoska, K., Likozar, B., & Novak, U. (2022). Permanent hydrophobic coating of chitosan/cellulose nanocrystals composite film by cold plasma processing. *Applied Surface Science, 597*, Article 153562. https://doi.org/10.1016/j.apsusc.2022.153562

Oliveri, P., Malegori, C., & Casale, M. (2020). Chemometrics: Multivariate analysis of chemical data. In *Chemical analysis of food* (pp. 33–76). Academic Press. https://doi.org/10.1016/B978-0-12-813266-1.00002-4.

Opwis, K., & Gutmann, J. S. (2011). Surface modification of textile materials with hydrophobins. *Textile Research Journal, 81*(15), 1594–1602. https://doi.org/10.1177/0040517511404599

Panieri, E., Baralic, K., Djukic-Cosic, D., Buha Djordjevic, A., & Saso, L. (2022). PFAS molecules: A major concern for the human health and the environment. *Toxics, 10*(2). https://doi.org/10.3390/toxics10020044

Peres-Neto, P. R., Legendre, P., Dray, S., & Borcard, D. (2006). Variation partitioning of species data matrices: Estimation and comparison of fractions. *Ecology, 87*(10), 2614–2625. https://doi.org/10.1890/0012-9658(2006)87[2614:VPOSDM]2.0.CO;2

Plate, S., Diekmann, S., Steinhäuser, U., & Drusch, S. (2012). Determination of the degree of substitution of hydrolysed octenylsuccinate-derivatised starch. *LWT - Food Science and Technology, 46*(2), 580–582. https://doi.org/10.1016/j.lwt.2011.12.014

Ren, L., Yan, X., Zhou, J., Tong, J., & Su, X. (2017). Influence of chitosan concentration on mechanical and barrier properties of corn starch/chitosan films. *International Journal of Biological Macromolecules, 105*, 1636–1643. https://doi.org/10.1016/j.ijbiomac.2017.02.008

Roy, S., Goh, K.-L., Verma, C., Dasgupta Ghosh, B., Sharma, K., & Maji, P. K. (2022). A facile method for processing durable and sustainable Superhydrophobic chitosan-based coatings derived from waste crab Shell. *ACS Sustainable Chemistry & Engineering, 10*(14), 4694–4704. https://doi.org/10.1021/acssuschemeng.2c00206

Saji, V. S. (2020). Wax-based artificial superhydrophobic surfaces and coatings. *Colloids and Surfaces A: Physicochemical and Engineering Aspects, 602*, Article 125132. https://doi.org/10.1016/j.colsurfa.2020.125132

Saleem, H., & Zaidi, S. J. (2020). Sustainable use of nanomaterials in textiles and their environmental impact. *Materials, 13*(22). https://doi.org/10.3390/ma13225134

Samanta, K. K., Gayatri, T. N., Basak, S., Chattopadhay, S. K., Arputharaj, A., & Prasad, V. (2016). Hydrophobic functionalization of cellulosic substrates using atmospheric pressure plasma. *Cellulose Chemistry and Technology, 50*(March 2017), 745–754.

Samanta, K. K., Joshi, A. G., Jassal, M., & Agrawal, A. K. (2021). Hydrophobic functionalization of cellulosic substrate by tetrafluoroethane dielectric barrier discharge plasma at atmospheric pressure. *Carbohydrate Polymers, 253*, Article 117272. https://doi.org/10.1016/j.carbpol.2020.117272

Shahid, M., Maiti, S., Adivarekar, R. V., & Liu, S. (2022). Biomaterial based fabrication of superhydrophobic textiles – A review. *Materials Today Chemistry, 24*, Article 100940. https://doi.org/10.1016/j.mtchem.2022.100940

Simončič, B., Hadžić, S., Vasiljević, J., Černe, L., Tomšič, B., Jerman, I., Orel, B., & Medved, J. (2014). Tailoring of multifunctional cellulose fibres with "lotus effect" and flame retardant properties. *Cellulose, 21*(1), 595–605. https://doi.org/10.1007/s10570-013-0103-4

Singh, A., Singh, M., Pandey, A., Ullas, A. V., & Mishra, S. (2023). Hydrophobicity of cotton fabric treated with plant extract, TiO2 nanoparticles and beeswax. *Materials Today Proceedings, 80*, 1530–1533. https://doi.org/10.1016/j.matpr.2023.01.353

Smith, T. W., & Lundholm, J. T. (2010). Variation partitioning as a tool to distinguish between niche and neutral processes. *Ecography, 33*(4), 648–655. https://doi.org/10.1111/j.1600-0587.2009.06105.x

Spyrakis, F., & Dragani, T. A. (2023). The EU's per- and polyfluoroalkyl substances (PFAS) ban: A case of policy over science. *Toxics, 11*(9). https://doi.org/10.3390/toxics11090721

Staneva, D., Atanasova, D., Angelova, D., Grozdanov, P., Nikolova, I., & Grabchev, I. (2023). Antimicrobial properties of chitosan-modified cotton fabric treated with aldehydes and zinc oxide particles. *Materials (Basel, Switzerland), 16*(14), 5090. https://doi.org/10.3390/ma16145090

Stres, B., Sul, W. J., Murovec, B., & Tiedje, J. M. (2013). Recently Deglaciated high-altitude soils of the Himalaya: Diverse environments, Heterogenous bacterial communities and long-range dust inputs from the upper troposphere. *PLoS One, 8*(9), Article e76440. https://doi.org/10.1371/journal.pone.0076440

Tagliaro, I., Mariani, M., Akbari, R., Contardi, M., Summa, M., Saliu, F., Nisticò, R., & Antonini, C. (2024). PFAS-free superhydrophobic chitosan coating for fabrics. *Carbohydrate Polymers, 333*, Article 121981. https://doi.org/10.1016/j.carbpol.2024.121981

Trubiano, P. C. (1986). Modified starches: Properties and uses. In *Succinate and substituted succinic derivatives of starch* (pp. 131–147). CRC Press. https://agris.fao.org/search/en/providers/123819/records/64735d1c2c1d629bc97cb031.

UNEP. (2009). *Decision SC-4/17. Listing of perfluorooctane sulfonic acid, its salts and perfluorooctane sulfonyl fluoride. UNEP-POPS-COP.4-SC-4-17* (conference of the parties to the Stockholm convention on persistent organic pollutants). http://chm.pops.int/TheConvention/ConferenceoftheParties/ReportsandDecisions/tabid/208/Default.aspx.

UNEP. (2019). *Decision SC-9/4. Perfluorooctane sulfonic acid, its salts and Perfluorooctane sulfonyl fluoride. UNEP-POPS-COP.9-SC-9-4* (conference of the parties to the Stockholm convention on persistent organic pollutants). http://www.pops.int/Implementation/IndustrialPOPs/PFOS/Decisions/tabid/5222/Default.aspx.

UNEP. (2022). *Decision SC-10/13. Listing of perfluorohexane sulfonic acid (PFHxS), its salts and PFHxS-related compounds. UNEP-POPS-COP.10-SC-10-3* (Conference of the parties to the Stockholm convention on persistent organic pollutants). https://chm.pops.int/TheConvention/ConferenceoftheParties/Meetings/COP10/tabid/8397/Default.aspx.

US EPA O. (2021, October 14). Our Current Understanding of the Human Health and Environmental Risks of PFAS [Overviews and Factsheets]. https://www.epa.gov/pfas/our-current-understanding-human-health-and-environmental-risks-pfas.

Verbič, A., Gorjanc, M., & Simončič, B. (2019). Zinc oxide for functional textile coatings: Recent advances. *Coatings, 9*(9). https://doi.org/10.3390/coatings9090550

Vidmar, B., Oberlintner, A., Stres, B., Likozar, B., & Novak, U. (2023). Biodegradation of polysaccharide-based biocomposites with acetylated cellulose nanocrystals, alginate and chitosan in aqueous environment. *International Journal of Biological Macromolecules, 252*, Article 126433. https://doi.org/10.1016/j.ijbiomac.2023.126433

Wang, L., Jia, Q., Li, Y., Zhao, H., & Wu, Z. (2025). Chitosan/OSA starch composite-stabilized Pickering emulsions: Characterization and its application in curcumin. *LWT, 222*, Article 117661. https://doi.org/10.1016/j.lwt.2025.117661

Xu, Y. X., Kim, K. M., Hanna, M. A., & Nag, D. (2005). Chitosan–starch composite film: Preparation and characterization. *Industrial Crops and Products, 21*(2), 185–192. https://doi.org/10.1016/j.indcrop.2004.03.002

Yan, C., McClements, D. J., Zhu, Y., Zou, L., Zhou, W., & Liu, W. (2019). Fabrication of OSA starch/chitosan polysaccharide-based high internal phase emulsion via altering interfacial behaviors. *Journal of Agricultural and Food Chemistry, 67*(39), 10937–10946. https://doi.org/10.1021/acs.jafc.9b04009

Ye, Z., Li, S., Zhao, S., Deng, L., Zhang, J., & Dong, A. (2021). Textile coatings configured by double-nanoparticles to optimally couple superhydrophobic and antibacterial properties. *Chemical Engineering Journal, 420*, Article 127680. https://doi.org/10.1016/j.cej.2020.127680

Zhang, F., Tao, H., Li, Y., Wang, Y., Zhou, Y., Xu, Q., & Ma, J. (2022). Enhanced pickering emulsion stabilization of cellulose nanocrystals and application for reinforced and hydrophobic coatings. *Coatings, 12*(10). https://doi.org/10.3390/coatings12101594

Zhao, S., Tian, G., Zhao, C., Lu, C., Bao, Y., Liu, X., & Zheng, J. (2018). Emulsifying stability properties of octenyl succinic anhydride (OSA) modified waxy starches with different molecular structures. *Food Hydrocolloids, 85*, 248–256. https://doi.org/10.1016/j.foodhyd.2018.07.029

Zheng, G., & Salamova, A. (2020). Are melamine and its derivatives the alternatives for per- and Polyfluoroalkyl substance (PFAS) fabric treatments in infant clothes? *Environmental Science & Technology, 54*(16), 10207–10216. https://doi.org/10.1021/acs.est.0c03035

Zhuo, L.-B., Liu, Y.-M., Jiang, Y., & Yan, Z. (2024). Zinc oxide nanoparticles induce acute lung injury via oxidative stress-mediated mitochondrial damage and NLRP3 inflammasome activation: In vitro and in vivo studies. *Environmental Pollution, 341*, Article 122950. https://doi.org/10.1016/j.envpol.2023.122950